Available online at www.sciencedirect.com
SCIENCE DIRECT®
ELSEVIER
Applied Mathematical Modelling 29 (2005) 754–783
APPLIED MATHEMATICAL MODELLING
www.elsevier.com/locate/apm

Numerical solution of the two-dimensional shallow water equations by the application of relaxation methods

A.I. Delis [a,*], Th. Katsaounis [b,c]

[a] *Division of Mathematics, Department of Sciences, Technical University of Crete, University Campus, Chania 73100, Crete, Greece*
[b] *Department of Applied Mathematics, University of Crete, Heraklion 71409, Crete, Greece*
[c] *Institute of Applied and Computational Mathematics, FORTH, Heraklion 71110, Crete, Greece*

Received 1 December 2003; received in revised form 1 October 2004; accepted 2 November 2004
Available online 20 December 2004

Abstract

A generalization and extension of a finite difference method for calculating numerical solutions of the two dimensional shallow water system of equations is investigated. A previously developed non-oscillatory relaxation scheme is generalized as to included problems with source terms in two dimensions, with emphasis given to the bed topography, resulting to a class of methods of first- and second-order in space and time. The methods are based on classical relaxation models combined with TVD Runge–Kutta time stepping mechanisms where neither Riemann solvers nor characteristic decompositions are needed. Numerical results are presented for several test problems with or without the source term present. The wetting and drying process is also considered. The presented schemes are verified by comparing the results with documented ones.

Keywords: Two-dimensional shallow water equations; Relaxation schemes; Finite differences; TVD; Source terms

* Correponding author. Fax: +30 28210 37842.
E-mail address: adelis@science.tuc.gr (A.I. Delis).

0307-904X/$ - see front matter
doi:10.1016/j.apm.2004.11.001

1. Introduction

During the past decades the shallow water model has been widely used to model physical phenomena of water flows such as, flood waves, dam-breaks, tidal flows in estuary and coastal water regions, and bore wave propagation in rivers, among others. Substantial effort has been devoted to the development of computational techniques for that kind of fluid flow simulations, and particular in the field of finite volumes for systems of conservation laws. There has been a growing trend in favor of Riemann or Godunov-type based methods constructed within the finite volume framework, see for example [37] and [24]. Such methods are noted for their good conservation and shock capturing capabilities. Higher order explicit and implicit TVD schemes for non-linear conservation laws utilize exact or approximate Riemann solvers and local characteristic decomposition when applied to the shallow water equations (SWEs), see for example [1,12,13,27–29,40,43], which theoretically can be rather complicated and expensive computationally. More recently many methods were proposed for the numerical approximation of solutions of hyperbolic conservations laws incorporating source terms, with application to the SWEs, based on such methods, see for example [4,5,11,16,31,39], producing very accurate results.

In general one can classify the different approaches as follows. The first class of methods, so-called upwind methods rely on approximate solutions of *non-linear Riemann problems*. This type of scheme go back to Godunov's original work. The second class are the *central schemes* and their new interpretation as Godunov-type schemes on *staggered grids*. A third approach to compute the non-linear fluxes is via *relaxation*. The concept is based on an approximation on the continuous level before any kind of discretization. This is a entirely different approach leading to high-resolution and Riemann-solver-free methods. This is important since in the case of complicated systems of conservation laws (for example in two-phase flow problems where in general we cannot expect to have an analytical expression for the physical flux or it is not possible to express the flux in terms of the conserved variables) when the Riemann problem is difficult to solve, even approximate solvers are difficult to use. The complexity increases even more for high resolution algorithms, where the unknowns are represented with higher order reconstructions. Such reconstructions should be applied to the local characteristic variables instead of the conserved ones, as to avoid oscillations on the numerical solution. Again, the computation of the characteristic variables is a local transformation which can be expensive to compute.

Relaxation schemes, as presented in [17], are based on a relaxation approximation to the non-linear conservation law, that has linear convection term and does not need a Riemann solver nor characteristic decomposition and thus enjoy great simplicity. This simplicity can be of great significance when one has to solve large scale engineering problems. The key issues, as pointed out in [30], is that *relaxation is a flux approximation* that formally can work for any flux function and that *relaxation linearizes the Riemann problem*. The above constitute relaxation approximations an alternative promising approach.

The purpose of the present work is to report on the applicability of recently developed relaxation algorithms, introduced in [14] for the one-dimensional case, in order to obtain numerical solutions for the two-dimensional SWEs. Thus far no application of relaxation schemes has been reported in solving two-dimensional shallow water problems. The class of relaxation schemes introduced in [17] has been subsequently widely studied but in a more theoretical context, see [2,3,7,8,10,19,22,21,26,33,36,38]. Recently in [23] the connection between a simple relaxation

scheme of the type proposed in [17] and a class of approximate Riemann solvers has been established. Using finite volume shock capturing spatial discretizations and a Runge–Kutta method to provide the time stepping mechanism, the proposed schemes combine simplicity and high efficiency and as thus can be considered as an alternative to finite volume methods based on approximate Riemann solvers. Their performance in various test problems shows that they can provide a reliable alternative for shallow water wave computations in two dimensions.

This paper is organized as follows: The two-dimensional SWEs are presented in Section 2. The relaxation systems for two different treatments of the geometrical source term for the SWEs are introduced in Section 3. The semi-discrete first and second-order schemes are presented in Section 4, and Section 5 is devoted in the presentation of the fully discrete schemes. Finally, in Section 6 a series of experiments displaying the features of the methods presented.

2. The 2D shallow water equations

The well known two-dimensional shallow water model, which represents mass and momentum conservation, can be obtained by depth averaging the Navier–Stokes equations. Neglecting diffusion of momentum due to viscosity and turbulence, wind effects and Coriolis terms, the model can be written in differential conservation law form as a single vector equation

$$\mathbf{U}_t + \mathbf{F}(\mathbf{U})_x + \mathbf{G}(\mathbf{U})_y = \mathbf{S}(\mathbf{U}); \quad (x,y) \in \Omega, \quad t \geqslant 0 \tag{2.1}$$

in which

$$\mathbf{U} = \begin{pmatrix} h \\ hu_1 \\ hu_2 \end{pmatrix} = \begin{pmatrix} h \\ q_1 \\ q_2 \end{pmatrix}, \quad \mathbf{S}(\mathbf{U}) = \begin{pmatrix} 0 \\ -gh\dfrac{\partial Z}{\partial x}(x,y) - ghS_{\mathrm{f}}^{x} \\ -gh\dfrac{\partial Z}{\partial y}(x,y) - ghS_{\mathrm{f}}^{y} \end{pmatrix},$$

$$\mathbf{F}(\mathbf{U}) = \begin{pmatrix} q_1 \\ \dfrac{q_1^2}{h} + \dfrac{1}{2}gh^2 \\ \dfrac{q_1 q_2}{h} \end{pmatrix}, \quad \mathbf{G}(\mathbf{U}) = \begin{pmatrix} q_2 \\ \dfrac{q_1 q_2}{h} \\ \dfrac{q_2^2}{h} + \dfrac{1}{2}gh^2 \end{pmatrix}.$$

System (2.1) describes the flow at time t at point $(x,y) \in \Omega$, where $h(x,y,t) \geqslant 0$ is the height of the fluid at point (x,y) at time t, Ω denotes the projection of the domain occupied by the fluid onto the x–y plane and $Z(x,y)$ is the bottom elevation function (bottom topography). The vector field (u_1,u_2) is the average velocity components, and g the gravitational acceleration. Finally, the conserved variable q (unit discharge) is given by $(q_1,q_2) = (hu_1,hu_2)$.

Source terms in the above shallow water system can be divide in two types: bed slopes in the x and y direction given by $-\partial Z/\partial x$, $-\partial Z/\partial y$, respectively and friction slopes S_{f}^{x} and S_{f}^{y} in the same directions. In the model, the friction slope can be estimated by using the empirical resistance relationships in the Manning form

$$S_f^x = n_m^2 u_1 \sqrt{u_1^2 + u_2^2} h^{-4/3}; \quad S_f^y = n_m^2 u_2 \sqrt{u_1^2 + u_2^2} h^{-4/3},$$

where n_m is the Manning roughness coefficient.

It is well known that the solutions of system (2.1) present steep fronts and shock discontinuities, which need to be resolved accurately in applications, and can cause severe numerical difficulties. Thus, computing numerical solutions of system (2.1) is not trivial due to non-linearity, the presence of the convective term and the coupling of the equations through the source term. The important part of the source term in that taken from the bottom topography and thus we will concentrate on that when creating relaxation models for the SWEs. On the other hand, the lack of spatial derivatives in the friction slopes makes its semi-implicit discretization practical. Friction terms in the SWEs are of relaxation type. However since Manning's coefficient is typically of order 10^{-2}, it can be verified (see [18]) that the related cell Peclet number is small and that the resulting relaxation terms are not stiff.

3. Relaxation systems for the 2D SWEs

Relaxation systems for the SWEs are motivated by the relaxation system of [17] for the 2-D scalar conservation laws. Consider the classical 2-D conservation law

$$\begin{aligned} &u_t + f(u)_x + g(u)_y = 0; \quad (x,y) \in \mathbb{R}^2, \ t > 0, \\ &u(x,y,0) = u_0(x,y); \quad (x,y) \in \mathbb{R}^2. \end{aligned} \tag{3.1}$$

Introducing the artificial variables v, w (relaxation variables) to (3.1), the linear relaxation system of [17] reads as follows:

$$\begin{aligned} &u_t + v_x + w_y = 0, \\ &v_t + c^2 u_x = -\frac{1}{\epsilon}(v - f(u)), \\ &w_t + d^2 u_y = -\frac{1}{\epsilon}(w - g(u)) \end{aligned} \tag{3.2}$$

with initial data

$$\begin{aligned} &u(x,y,0) = u_0(x,y), \\ &v(x,y,0) = v_0(x,y) = f(u_0(x,y)), \\ &w(x,y,0) = w_0(x,y) = g(u_0(x,y)), \end{aligned}$$

where the small parameter ϵ is the *relaxation rate* ($0 < \epsilon \ll 1$) and c,d positive constants. System (3.2) is dissipative under the following *subcharateristic condition*

$$\frac{f'(u)^2}{c^2} + \frac{g'(u)^2}{d^2} \leqslant 1 \quad \forall u, \tag{3.3}$$

and guarantees that system (3.2) is non-linearly stable, and then in the small relaxation limit $\epsilon \to 0^+$ we recover (3.1).

Following the previous motivation and the works in [14] and [20], we generalize and extend the relaxation system for the SWEs in 2D with the topography source term present, replacing the conservation law (2.1) by the larger system

$$h_t + v_{1x} + w_{1y} = 0, \tag{3.4a}$$

$$q_{1t} + v_{2x} + w_{2y} = -ghZ_x, \tag{3.4b}$$

$$q_{2t} + v_{3x} + w_{3y} = -ghZ_y, \tag{3.4c}$$

$$v_{1t} + c_1^2 h_x = -\frac{1}{\epsilon}(v_1 - q_1), \tag{3.4d}$$

$$v_{2t} + c_2^2 q_{1x} = -\frac{1}{\epsilon}\left(v_2 - \left(\frac{q_1^2}{h} + \frac{g}{2}h^2\right)\right), \tag{3.4e}$$

$$v_{3t} + c_3^2 q_{2x} = -\frac{1}{\epsilon}\left(v_3 - \left(\frac{q_1 q_2}{h}\right)\right), \tag{3.4f}$$

$$w_{1t} + d_1^2 h_y = -\frac{1}{\epsilon}(w_1 - q_2), \tag{3.4g}$$

$$w_{2t} + d_2^2 q_{1y} = -\frac{1}{\epsilon}\left(w_2 - \left(\frac{q_1 q_2}{h}\right)\right), \tag{3.4h}$$

$$w_{3t} + d_3^2 q_{2y} = -\frac{1}{\epsilon}\left(w_3 - \left(\frac{q_2^2}{h} + \frac{g}{2}h^2\right)\right). \tag{3.4i}$$

Setting now

$$\mathbf{u} = \begin{bmatrix} h \\ q_1 \\ q_2 \end{bmatrix}, \quad \mathbf{v} = \begin{bmatrix} v_1 \\ v_2 \\ v_3 \end{bmatrix}, \quad \mathbf{w} = \begin{bmatrix} w_1 \\ w_2 \\ w_3 \end{bmatrix}, \tag{3.5}$$

system (3.4) can be rewritten as

$$\begin{aligned} &\mathbf{u}_t + \mathbf{v}_x + \mathbf{w}_y = \mathbf{S}(\mathbf{u}), \\ &\mathbf{v}_t + \mathbf{C}^2\mathbf{u}_x = -\frac{1}{\epsilon}(\mathbf{v} - \mathbf{F}(\mathbf{u})) \\ &\mathbf{w}_t + \mathbf{D}^2\mathbf{u}_y = -\frac{1}{\epsilon}(\mathbf{w} - \mathbf{G}(\mathbf{u})), \end{aligned} \tag{3.6}$$

where now $\mathbf{u}, \mathbf{v}, \mathbf{w} \in \mathbb{R}^3$ and $\mathbf{C}^2, \mathbf{D}^2 \in \mathbb{R}^{3\times 3}$ are positive diagonal matrices. We assume without loss of generality that $\mathbf{C}$,$\mathbf{D}$ have positive eigenvalues c_j, $d_j > 0$ for $j = 1, 2, 3$. Consequently, in the limit $\epsilon \to 0^+$ system (3.6) approaches the original system (2.1) by the *local equilibrium* $\mathbf{v} = \mathbf{F}(\mathbf{u})$ and $\mathbf{w} = \mathbf{G}(\mathbf{u})$.

System (3.6) can now be further reformulated as

$$\begin{bmatrix} \mathbf{u} \\ \mathbf{v} \\ \mathbf{w} \end{bmatrix}_t + \begin{bmatrix} 0 & \mathbf{I} & 0 \\ \mathbf{C}^2 & 0 & 0 \\ 0 & 0 & 0 \end{bmatrix} \begin{bmatrix} \mathbf{u} \\ \mathbf{v} \\ \mathbf{w} \end{bmatrix}_x + \begin{bmatrix} 0 & 0 & \mathbf{I} \\ 0 & 0 & 0 \\ \mathbf{D}^2 & 0 & 0 \end{bmatrix} \begin{bmatrix} \mathbf{u} \\ \mathbf{v} \\ \mathbf{w} \end{bmatrix}_y = \begin{bmatrix} \mathbf{S}(\mathbf{u}) \\ -\frac{1}{\epsilon}(\mathbf{v} - \mathbf{F}(\mathbf{u})) \\ -\frac{1}{\epsilon}(\mathbf{w} - \mathbf{G}(\mathbf{u})) \end{bmatrix}. \tag{3.7}$$

We also consider the following two novel variants, of the above relaxation system:

$$h_t + v_{1x} + w_{1y} = 0, \tag{3.8a}$$

$$q_{1t} + v_{2x} + w_{2y} = 0, \tag{3.8b}$$

$$q_{2t} + v_{3x} + w_{3y} = 0, \tag{3.8c}$$

$$v_{1t} + c_1^2 h_x = -\frac{1}{\epsilon}(v_1 - q_1), \tag{3.8d}$$

$$v_{2t} + c_2^2 q_{1x} = -\frac{1}{\epsilon}\left(v_2 - \left(\frac{q_1^2}{h} + \frac{g}{2}h^2\right)\right) + \frac{1}{2}\frac{1}{\epsilon}\int^x gh(s,y)\frac{\partial Z}{\partial x}(s,y)\,\mathrm{d}s, \tag{3.8e}$$

$$v_{3t} + c_3^2 q_{2x} = -\frac{1}{\epsilon}\left(v_3 - \left(\frac{q_1 q_2}{h}\right)\right) + \frac{1}{2}\frac{1}{\epsilon}\int^x gh(s,y)\frac{\partial Z}{\partial y}(s,)\,\mathrm{d}s, \tag{3.8f}$$

$$w_{1t} + d_1^2 h_y = -\frac{1}{\epsilon}(w_1 - q_2), \tag{3.8g}$$

$$w_{2t} + d_2^2 q_{1y} = -\frac{1}{\epsilon}\left(w_2 - \left(\frac{q_1 q_2}{h}\right)\right) + \frac{1}{2}\frac{1}{\epsilon}\int^y gh(x,s)\frac{\partial Z}{\partial x}(x,s)\,\mathrm{d}s, \tag{3.8h}$$

$$w_{3t} + d_3^2 q_{2y} = -\frac{1}{\epsilon}\left(w_3 - \left(\frac{q_2^2}{h} + \frac{g}{2}h^2\right)\right) + \frac{1}{2}\frac{1}{\epsilon}\int^y gh(x,s)\frac{\partial Z}{\partial y}(x,s)\,\mathrm{d}s, \tag{3.8i}$$

and the alternative form

$$h_t + v_{1x} + w_{1y} = 0, \tag{3.9a}$$

$$q_{1t} + v_{2x} + w_{2y} = 0, \tag{3.9b}$$

$$q_{2t} + v_{3x} + w_{3y} = 0, \tag{3.9c}$$

$$v_{1t} + c_1^2 h_x = -\frac{1}{\epsilon}(v_1 - q_1), \tag{3.9d}$$

$$v_{2t} + c_2^2 q_{1x} = -\frac{1}{\epsilon}\left(v_2 - \left(\frac{q_1^2}{h} + \frac{g}{2}h^2\right)\right) + \frac{1}{\epsilon}\int^x gh(s,y)\frac{\partial Z}{\partial x}(s,y)\,\mathrm{d}s, \tag{3.9e}$$

$$v_{3t} + c_3^2 q_{2x} = -\frac{1}{\epsilon}\left(v_3 - \left(\frac{q_1 q_2}{h}\right)\right), \tag{3.9f}$$

$$w_{1t} + d_1^2 h_y = -\frac{1}{\epsilon}(w_1 - q_2), \tag{3.9g}$$

$$w_{2t} + d_2^2 q_{1y} = -\frac{1}{\epsilon}\left(w_2 - \left(\frac{q_1 q_2}{h}\right)\right), \tag{3.9h}$$

$$w_{3t} + d_3^2 q_{2y} = -\frac{1}{\epsilon}\left(w_3 - \left(\frac{q_2^2}{h} + \frac{g}{2}h^2\right)\right) + \frac{1}{\epsilon}\int^y gh(x,s)\frac{\partial Z}{\partial y}(x,s)\,\mathrm{d}s, \tag{3.9i}$$

written in vector form as

$$\begin{bmatrix}\mathbf{u}\\ \mathbf{v}\\ \mathbf{w}\end{bmatrix}_t + \begin{bmatrix}0 & \mathbf{I} & 0\\ \mathbf{C}^2 & 0 & 0\\ 0 & 0 & 0\end{bmatrix}\begin{bmatrix}\mathbf{u}\\ \mathbf{v}\\ \mathbf{w}\end{bmatrix}_x + \begin{bmatrix}0 & 0 & \mathbf{I}\\ 0 & 0 & 0\\ \mathbf{D}^2 & 0 & 0\end{bmatrix}\begin{bmatrix}\mathbf{u}\\ \mathbf{v}\\ \mathbf{w}\end{bmatrix}_y = \begin{bmatrix}0\\ -\frac{1}{\epsilon}(\mathbf{v} - \mathbf{F}(\mathbf{u})) - \frac{1}{\epsilon}\widetilde{\mathbf{S}}(\mathbf{u})\\ -\frac{1}{\epsilon}(\mathbf{w} - \mathbf{G}(\mathbf{u})) - \frac{1}{\epsilon}\widetilde{\widetilde{\mathbf{S}}}(\mathbf{u})\end{bmatrix}, \tag{3.10}$$

where

$$\widetilde{\mathbf{S}}(\mathbf{u}) = \begin{bmatrix}0\\ -\int^x gh(s,y)\frac{\partial Z}{\partial x}(s,y)\,\mathrm{d}s\\ 0\end{bmatrix} \quad \text{and} \quad \widetilde{\widetilde{\mathbf{S}}}(\mathbf{u}) = \begin{bmatrix}0\\ 0\\ -\int^y gh(x,s)\frac{\partial Z}{\partial y}(x,s)\,\mathrm{d}s\end{bmatrix}$$

or

$$\widetilde{\mathbf{S}}(\mathbf{u}) = \begin{bmatrix}0\\ -\frac{1}{2}\int^x gh(s,y)\frac{\partial Z}{\partial x}(s,y)\,\mathrm{d}s\\ -\frac{1}{2}\int^x gh(s,y)\frac{\partial Z}{\partial y}(s,y)\,\mathrm{d}s\end{bmatrix} \quad \text{and} \quad \widetilde{\widetilde{\mathbf{S}}}(\mathbf{u}) = \begin{bmatrix}0\\ -\frac{1}{2}\int^y gh(x,s)\frac{\partial Z}{\partial x}(x,s)\,\mathrm{d}s\\ -\frac{1}{2}\int^y gh(x,s)\frac{\partial Z}{\partial y}(x,s)\,\mathrm{d}s\end{bmatrix}.$$

Relaxation system (3.10) approaches, in the limit, the original system (2.1) by the local equilibrium

$$\mathbf{v} = \mathbf{F}(\mathbf{u}) - \widetilde{\mathbf{S}}(\mathbf{u}) \quad \text{and} \quad \mathbf{w} = \mathbf{G}(\mathbf{u}) - \widetilde{\widetilde{\mathbf{S}}}(\mathbf{u}).$$

The original conservation law, in all formulations, has now been replaced by a linear hyperbolic system with a relaxation source term which rapidly drives to local equilibriums in the relaxation limit $\epsilon \to 0^+$. In some cases it can be shown analytically that solutions to (3.7) approach solutions to the original conservation law. See for example [9,25,30,42,38,41], for discussions of this condition and convergence properties.

A general necessary condition for such convergence is that the subcharacteristic condition is satisfied. For systems (3.7), (3.10) we require that

$$\frac{\lambda_i^2}{c_i^2} + \frac{\mu_i^2}{d_i^2} \leqslant 1 \quad \forall i = 1,2,3 \tag{3.11}$$

with λ_i, μ_i being the eigenvalues of $\partial\mathbf{F}(\mathbf{u})/\partial\mathbf{u}$ and $\partial\mathbf{G}(\mathbf{u})/\partial\mathbf{u}$, respectively. By doing so we insure that the characteristic speeds of the hyperbolic part of (3.7) or (3.10) are at least as large as the characteristic speeds of the original problem. Hence, by choosing the constants c_i,d_i appropriately, so that the subcharacteristic condition hold true, in the relaxation limit $\epsilon \to 0^+$ we recover (2.1), for both relaxation systems (3.7) and (3.10).

4. Semi-discrete relaxation schemes

We start first with the semi-discrete schemes for the relaxation systems (3.7) and (3.10). We consider a classical first-order upwind scheme and a second-order MUSCL scheme. For brevity we present the semi-discrete schemes for system (3.10). Since the relaxation system has linear convection terms, it is rather simple to employ an upwind scheme, in contrast to a non-linear system of conservation laws where in an upwind scheme the use of a Riemann solver and local characteristic decomposition are necessary. The relaxation scheme treats the spatial and time discretization separately.

To discretize the system of equations, a spatially 2D domain of integration, divided into cells (i,j), is assumed, with a uniform grid widths in each direction, $\Delta x = x_{i+\frac{1}{2}} - x_{i-\frac{1}{2}}$, $\Delta y = y_{i+\frac{1}{2}} - y_{i-\frac{1}{2}}$ and a uniform time step $\Delta t = t^{n+1} - t^n$, $n = 0, 1, 2, \ldots$. The approximate solution, denoted as the discrete value $\mathbf{u}_{ij}^n$, is the approximate cell average of the variable $\mathbf{u}$ in the cell $(x_{i+\frac{1}{2}}, x_{i-\frac{1}{2}}) \times (y_{i+\frac{1}{2}}, y_{i-\frac{1}{2}})$ at time $t = t^n$. The approximate point value of $\mathbf{u}$ at $(x, y) = (x_{i+\frac{1}{2}}, y_{j+\frac{1}{2}})$ at time $t = t^n$ is denoted by $\mathbf{u}^n_{i+\frac{1}{2},j+\frac{1}{2}}$.

4.1. The upwind scheme

We start by considering the following one-step conservative system for the homogeneous case (no source term is present)

$$\begin{aligned}
&\frac{\partial}{\partial t}\mathbf{u}_{ij} + \frac{1}{\Delta x}(\mathbf{v}_{i+\frac{1}{2},j} - \mathbf{v}_{i-\frac{1}{2},j}) + \frac{1}{\Delta y}(\mathbf{w}_{i,j+\frac{1}{2},} - \mathbf{w}_{i,j-\frac{1}{2}}) = 0,\\
&\frac{\partial}{\partial t}\mathbf{v}_{ij} + \frac{1}{\Delta x}\mathbf{C}^2(\mathbf{u}_{i+\frac{1}{2},j} - \mathbf{u}_{i-\frac{1}{2},j}) = -\frac{1}{\epsilon}(\mathbf{v}_{ij} - \mathbf{F}(\mathbf{u}_{ij})),\\
&\frac{\partial}{\partial t}\mathbf{w}_{ij} + \frac{1}{\Delta y}\mathbf{D}^2(\mathbf{u}_{i,j+\frac{1}{2}} - \mathbf{u}_{i,j-\frac{1}{2}}) = -\frac{1}{\epsilon}(\mathbf{w}_{ij} - \mathbf{G}(\mathbf{u}_{ij})).
\end{aligned} \tag{4.1}$$

The linear hyperbolic part of the (4.1) has two Riemann invariants (characteristic speeds) in each direction, $\mathbf{v} \pm \mathbf{Cu}$ in the x-direction and $\mathbf{w} \pm \mathbf{Du}$ in the y-direction, associated with the characteristic fields $\pm\mathbf{C}$ and $\pm\mathbf{D}$, respectively. The first-order upwind scheme applied to $\mathbf{v} \pm \mathbf{Cu}$ and $\mathbf{w} \pm \mathbf{Du}$ gives

$$\begin{aligned}
&(\mathbf{v} + \mathbf{Cu})_{i+\frac{1}{2},j} = (\mathbf{v} + \mathbf{Cu})_{ij}, \quad (\mathbf{v} - \mathbf{Cu})_{i+\frac{1}{2},j} = (\mathbf{v} - \mathbf{Cu})_{i+1,j},\\
&(\mathbf{w} + \mathbf{Du})_{i,j+\frac{1}{2}} = (\mathbf{w} + \mathbf{Du})_{ij}, \quad (\mathbf{w} - \mathbf{Du})_{i,j+\frac{1}{2}} = (\mathbf{w} - \mathbf{Du})_{i,j+1}.
\end{aligned} \tag{4.2}$$

Hence,

$$\begin{aligned}
\mathbf{u}_{i+\frac{1}{2},j} &= \frac{1}{2}(\mathbf{u}_{ij} + \mathbf{u}_{i+1,j}) - \frac{1}{2}\mathbf{C}^{-1}(\mathbf{v}_{i+1,j} - \mathbf{v}_{ij}),\\
\mathbf{v}_{i+\frac{1}{2},j} &= \frac{1}{2}(\mathbf{v}_{ij} + \mathbf{v}_{i+1,j}) - \frac{1}{2}\mathbf{C}(\mathbf{u}_{i+1,j} - \mathbf{u}_{ij}),\\
\mathbf{u}_{i,j+\frac{1}{2}} &= \frac{1}{2}(\mathbf{u}_{ij} + \mathbf{u}_{i,j+1}) - \frac{1}{2}\mathbf{D}^{-1}(\mathbf{w}_{i,j+1} - \mathbf{w}_{ij}),\\
\mathbf{w}_{i,j+\frac{1}{2}} &= \frac{1}{2}(\mathbf{w}_{ij} + \mathbf{w}_{i,j+1}) - \frac{1}{2}\mathbf{D}(\mathbf{u}_{i,j+1} - \mathbf{u}_{ij}).
\end{aligned} \tag{4.3}$$

We can then construct the following first-order upwind semi-discrete approximation of the relaxation scheme (3.10):

$$\begin{aligned}
&\frac{\partial}{\partial t}\mathbf{u}_{ij} + \frac{(\mathbf{v}_{i+1,j} - \mathbf{v}_{i-1,j})}{2\Delta x} + \frac{(\mathbf{w}_{i,j+1} - \mathbf{w}_{i,j-1})}{2\Delta y} - \frac{\mathbf{C}(\mathbf{u}_{i+1,j} - 2\mathbf{u}_{ij} + \mathbf{u}_{i-1,j})}{2\Delta x}\\
&\quad - \frac{\mathbf{D}(\mathbf{u}_{i,j+1} - 2\mathbf{u}_{ij} + \mathbf{u}_{i,j-1})}{2\Delta y} = 0,\\
&\frac{\partial}{\partial t}\mathbf{v}_{ij} + \frac{\mathbf{C}^2(\mathbf{u}_{i+1,j} - \mathbf{u}_{i-1,j})}{2\Delta x} - \frac{\mathbf{C}(\mathbf{v}_{i+1,j} - 2\mathbf{v}_{ij} + \mathbf{v}_{i-1,j})}{2\Delta x} = -\frac{1}{\epsilon}(\mathbf{v}_{ij} - \mathbf{F}(\mathbf{u}_{ij})) - \frac{1}{\epsilon}\widetilde{\mathbf{S}}(\mathbf{u}_{ij}),\\
&\frac{\partial}{\partial t}\mathbf{w}_{ij} + \frac{\mathbf{D}^2(\mathbf{u}_{i,j+1} - \mathbf{u}_{i,j-1})}{2\Delta y} - \frac{\mathbf{D}(\mathbf{w}_{i,j+1} - 2\mathbf{w}_{ij} + \mathbf{w}_{i,j-1})}{2\Delta y} = -\frac{1}{\epsilon}(\mathbf{w}_{ij} - \mathbf{G}(\mathbf{u}_{ij})) - \frac{1}{\epsilon}\widetilde{\widetilde{\mathbf{S}}}(\mathbf{u}_{ij}).
\end{aligned} \tag{4.4}$$

where $\widetilde{\mathbf{S}}, \widetilde{\widetilde{\mathbf{S}}}$ as defined for the system (3.10).

4.2. A MUSCL scheme

To construct a second-order accurate in space scheme, the piecewise constant approximation (4.2) is replaced with an MUSCL piecewise linear interpolation which, applied to the kth component of $\mathbf{v} \pm \mathbf{C}\mathbf{u}$, gives, respectively:

$$\begin{aligned}
(v + c_k u)_{i+\frac{1}{2},j} &= (v + c_k u)_{ij} + \frac{1}{2}\Delta x s_{ij}^{x,+},\\
(v - c_k u)_{i+\frac{1}{2},j} &= (v - c_k u)_{i+1,j} - \frac{1}{2}\Delta x s_{i+1,j}^{x,-},\\
(w + d_k u)_{i,j+\frac{1}{2}} &= (w + d_k u)_{ij} + \frac{1}{2}\Delta y s_{ij}^{y,+},\\
(w - d_k u)_{i,j+\frac{1}{2}} &= (v - d_k u)_{i,j+1} - \frac{1}{2}\Delta y s_{i,j+1}^{y-},
\end{aligned} \tag{4.5}$$

where u, v and w are the kth ($1 \leqslant k \leqslant 3$ for the SWEs) components of $\mathbf{v}$,$\mathbf{u}$ and $\mathbf{w}$, respectively, with s being the slopes in the (i,j)th cell, defined as

$$s_{ij}^{x,\pm} = \frac{1}{\Delta x}(v_{i+1,j} \pm c_k u_{i+1,j} - v_{ij} \mp c_k u_{ij})\phi(\theta_{ij}^{x,\pm}) \tag{4.6}$$

with

$$\theta_{ij}^{x,\pm} = \frac{v_{ij} \pm c_k u_{ij} - v_{i-1,j} \mp c_k u_{i-1,j}}{v_{i+1,j} \pm c_k u_{i+1,j} - v_{i,j} \mp c_k u_{ij}} \tag{4.7}$$

and

$$s_{ij}^{y,\pm} = \frac{1}{\Delta y}(w_{i,j+1} \pm d_k u_{i,j+1} - w_{ij} \mp d_k u_{ij})\phi(\theta_{ij}^{y,\pm}) \tag{4.8}$$

with

$$\theta_{ij}^{y,\pm} = \frac{w_{ij} \pm d_k u_{ij} - w_{i,j-1} \mp d_k u_{i,j-1}}{w_{i,j+1} \pm d_k u_{i,j+1} - w_{i,j} \mp d_k u_{ij}}, \tag{4.9}$$

where ϕ is a *limiter function*, as defined for example by Sweby [35], satisfying

$$0 \leqslant \phi(\theta) \leqslant \text{Min Mod}(2, 2\theta).$$

There are several options on choosing a limiter function. Some of the most popular ones are, the Min Mod (MM) limiter

$$\phi(\theta) = \max(0, \min(1, \theta)),$$

the Superbee (SB) limiter

$$\phi(\theta) = \max(0, \min(2\theta, 1), \min(\theta, 2)),$$

the VanLeer (VL) limiter

$$\phi(\theta) = \frac{|\,\theta\,| + \theta}{1 + |\,\theta\,|},$$

and the monotonized central (MC) limiter

$$\phi(\theta) = \max(0, \min((1+\theta)/2, 2, 2\theta)).$$

The last three limiters have been shown to exhibit sharper resolution of discontinuities, since they do not reduce the slope as severely as MM near a discontinuity.

Following from (4.5) we get:

$$\begin{aligned} u_{i+\frac{1}{2},j} &= \frac{1}{2}(u_{ij} + u_{i+1,j}) - \frac{1}{2c_k}(v_{i+1,j} - v_{ij}) + \frac{\Delta x}{4c_k}(s_{ij}^{x,+} + s_{i+1,j}^{x,-}), \\ v_{i+\frac{1}{2},j} &= \frac{1}{2}(v_{ij} + v_{i+1,j}) - \frac{c_k}{2}(u_{i+1,j} - u_{ij}) + \frac{\Delta x}{4}(s_{ij}^{x,+} - s_{i+1,j}^{x,-}), \end{aligned} \tag{4.10}$$

$$\begin{aligned} u_{i,j+\frac{1}{2}} &= \frac{1}{2}(u_{ij} + u_{i,j+1}) - \frac{1}{2d_k}(w_{i,j+1} - w_{ij}) + \frac{\Delta y}{4d_k}(s_{ij}^{y,+} + s_{i,j+1}^{y,-}), \\ w_{i,j+\frac{1}{2}} &= \frac{1}{2}(w_{ij} + w_{i,j+1}) - \frac{d_k}{2}(u_{i,j+1} - u_{ij}) + \frac{\Delta y}{4}(s_{ij}^{y,+} - s_{i,j+1}^{y,-}). \end{aligned} \tag{4.11}$$

Then the second-order (in space) semi-discrete relaxation scheme is given componentwise by

$$\begin{aligned}
&\frac{\partial}{\partial t}u_{ij}+\frac{1}{2\Delta x}(v_{i+1,j}-v_{i-1,j})-\frac{c_k}{2\Delta x}(u_{i+1,j}-2u_{ij}+u_{i-1,j})-\frac{d_k}{2\Delta y}(w_{i,j+1}-2w_{ij}+w_{i,j-1})\\
&\quad+\frac{1}{4}(s^{x,+}_{ij}-s^{x,-}_{i+1,j}-s^{x,+}_{i-1,j}+s^{x,-}_{ij}+s^{y,+}_{ij}-s^{y,-}_{i,j+1}-s^{y,+}_{i,j-1}+s^{y,-}_{ij})=0,\\
&\frac{\partial}{\partial t}v_{ij}+\frac{c_k^2}{2\Delta x}(u_{i+1,j}-u_{i-1,j})-\frac{c_k}{2\Delta x}(v_{i+1,j}-2v_{ij}+v_{i-1,j})\\
&\quad+\frac{c_k}{4}(s^{x,+}_{ij}+s^{x,-}_{i+1,j}-s^{x,+}_{i-1,j}-s^{x,-}_{ij})=-\frac{1}{\epsilon}(v_{ij}-F_k(u_{ij}))-\frac{1}{\epsilon}\widetilde{S}_k(u_{ij}),\\
&\frac{\partial}{\partial t}w_{ij}+\frac{d_k^2}{2\Delta y}(u_{i,j+1}-u_{i,j-1})-\frac{d_k}{2\Delta y}(w_{i,j+1}-2w_{ij}+v_{i,j-1})\\
&\quad+\frac{d_k}{4}(s^{y,+}_{ij}+s^{y,-}_{i+1,j}-s^{y,+}_{i-1,j}-s^{y,-}_{ij})=-\frac{1}{\epsilon}(w_{ij}-G_k(u_{ij}))-\frac{1}{\epsilon}\widetilde{\widetilde{S}}_k(u_{ij})
\end{aligned}\tag{4.12}$$

with $\widetilde{S}_k, \widetilde{\widetilde{S}}_k, F_k, G_k$ being the kth components of $\widetilde{\mathbf{S}}, \widetilde{\widetilde{\mathbf{S}}}, \mathbf{F}$ and $\mathbf{G}$, respectively. Notice that in the case the slope $s^{\pm}=0$ or $\phi=0$, the MUSCL scheme (4.12) reduces to the upwind scheme (4.4).

5. Fully discrete schemes

In this section we present the time discretization of the semi-discrete relaxation schemes applied to the SWEs. The obvious advantage of the relaxation approximation is that partial differential operator is linear and can easily diagonalized. Moreover, the ODE determined by the right side is a stiff but linear system, note that $\mathbf{u}_t=0$ and thus implicit methods can be applied without solving linear systems of equations. That is what makes numerical schemes based on relaxation so attractive. We will compare the two space discretization, upwind and MUSCL, applying an implicit Runge–Kutta method as the time marching mechanism to advance the solution by one time step Δt. To simplify the presentation we assume that $Z\equiv 0$, then

(A) Given $\mathbf{u}^n, \mathbf{v}^n, \mathbf{w}^n$ apply a finite volume method to update $\mathbf{u}$, $\mathbf{v}$ and $\mathbf{w}$ over time Δt by solving the homogeneous linear hyperbolic system

$$\begin{bmatrix}\mathbf{u}\\ \mathbf{v}\\ \mathbf{w}\end{bmatrix}_t+\begin{bmatrix}0 & \mathbf{I} & 0\\ \mathbf{C}^2 & 0 & 0\\ 0 & 0 & 0\end{bmatrix}\begin{bmatrix}\mathbf{u}\\ \mathbf{v}\\ \mathbf{w}\end{bmatrix}_x+\begin{bmatrix}0 & 0 & \mathbf{I}\\ 0 & 0 & 0\\ \mathbf{D}^2 & 0 & 0\end{bmatrix}\begin{bmatrix}\mathbf{u}\\ \mathbf{v}\\ \mathbf{w}\end{bmatrix}_y=\begin{bmatrix}0\\ 0\\ 0\end{bmatrix}.\tag{5.1}$$

and obtain new values $\mathbf{u}^{(1)}$, $\mathbf{v}^{(1)}$ and $w^{(1)}$.

(B) Update $\mathbf{u}^{(1)}$, $\mathbf{v}^{(1)}$, $\mathbf{w}^{(1)}$ to $\mathbf{u}^{n+1}$, $\mathbf{v}^{n+1}$, $\mathbf{w}^{n+1}$ by solving the equations

$$\begin{aligned}
&\mathbf{u}_t=0,\\
&\mathbf{v}_t=-\frac{1}{\epsilon}(\mathbf{v}-\mathbf{F}(\mathbf{u})),\\
&\mathbf{w}_t=-\frac{1}{\epsilon}(\mathbf{w}-\mathbf{G}(\mathbf{u})),
\end{aligned}\tag{5.2}$$

over time Δt.

A second-order implicit–explicit (IMEX) Runge–Kutta splitting scheme was introduced in [17] and is utilized here for both source term formulations. The splitting treats, alternatively, the stiff source terms $\frac{1}{\epsilon}(\mathbf{v}-\mathbf{F}(\mathbf{u}))$ and $\frac{1}{\epsilon}(\mathbf{w}-\mathbf{G}(\mathbf{u}))$ implicitly in two steps (that due to linearity of $\mathbf{v}$ and $\mathbf{w}$ one still solve them explicitly), and the convection terms with two explicit steps. Thus, we have an explicit implementation of an implicit source term, with stability constraints solely determined by the non-stiff convection terms, just as in a usual shock capturing scheme.

For the first source term application, corresponding to system (3.7), and temporarily dropping the subscript indices, given $\{\mathbf{u}^n,\mathbf{v}^n\mathbf{w}^n\}$, then $\{\mathbf{u}^{n+1},\mathbf{v}^{n+1}\mathbf{w}^{n+1}\}$ are computed by

$$\mathbf{u}^{n,1}=\mathbf{u}^n, \tag{5.3a}$$

$$\mathbf{v}^{n,1}=\mathbf{v}^n+\frac{\Delta t}{\epsilon}(\mathbf{v}^{n,1}-\mathbf{F}(\mathbf{u}^{n,1})), \tag{5.3b}$$

$$\mathbf{w}^{n,1}=\mathbf{w}^n+\frac{\Delta t}{\epsilon}(\mathbf{w}^{n,1}-\mathbf{G}(\mathbf{u}^{n,1})); \tag{5.3c}$$

$$\mathbf{u}^{(1)}=\mathbf{u}^{n,1}-\Delta t(\Delta_+^x\mathbf{v}^{n,1}+\Delta_+^y\mathbf{w}^{n,1})+\Delta t\mathbf{S}(\mathbf{u}^{n,1}), \tag{5.3d}$$

$$\mathbf{v}^{(1)}=\mathbf{v}^{n,1}-\Delta t\mathbf{C}^2\Delta_+^x\mathbf{u}^{n,1}, \tag{5.3e}$$

$$\mathbf{w}^{(1)}=\mathbf{w}^{n,1}-\Delta t\mathbf{D}^2\Delta_+^y\mathbf{u}^{n,1}; \tag{5.3f}$$

$$\mathbf{u}^{n,2}=\mathbf{u}^{(1)}, \tag{5.3g}$$

$$\mathbf{v}^{n,2}=\mathbf{v}^{(1)}-\frac{\Delta t}{\epsilon}(\mathbf{v}^{n,2}-\mathbf{F}(\mathbf{u}^{n,2}))-\frac{2\Delta t}{\epsilon}(\mathbf{v}^{n,1}-\mathbf{F}(\mathbf{u}^{n,1})), \tag{5.3h}$$

$$\mathbf{w}^{n,2}=\mathbf{w}^{(1)}-\frac{\Delta t}{\epsilon}(\mathbf{w}^{n,2}-\mathbf{G}(\mathbf{u}^{n,2}))-\frac{2\Delta t}{\epsilon}(\mathbf{w}^{n,1}-\mathbf{G}(\mathbf{u}^{n,1})); \tag{5.3i}$$

$$\mathbf{u}^{(2)}=\mathbf{u}^{n,2}-\Delta t(\Delta_+^x\mathbf{v}^{n,2}+\Delta_+^y\mathbf{w}^{n,2})+\Delta t\mathbf{S}(\mathbf{u}^{n,2}), \tag{5.3j}$$

$$\mathbf{v}^{(2)}=\mathbf{v}^{n,2}-\Delta t\mathbf{C}^2\Delta_+^x\mathbf{u}^{n,2}, \tag{5.3k}$$

$$\mathbf{w}^{(2)}=\mathbf{w}^{n,2}-\Delta t\mathbf{D}^2\Delta_+^y\mathbf{u}^{n,2}; \tag{5.3l}$$

$$\mathbf{u}^{n+1}=\frac{1}{2}(\mathbf{u}^n+\mathbf{u}^{(2)}), \tag{5.3m}$$

$$\mathbf{v}^{n+1}=\frac{1}{2}(\mathbf{v}^n+\mathbf{v}^{(2)}), \tag{5.3n}$$

$$\mathbf{w}^{n+1}=\frac{1}{2}(\mathbf{w}^n+\mathbf{w}^{(2)}), \tag{5.3o}$$

where

$$\Delta_+^x \mathbf{p}_{ij} = \frac{1}{\Delta x}(\mathbf{p}_{i+\frac{1}{2},j} - \mathbf{p}_{i-\frac{1}{2},j})$$

and

$$\Delta_+^y \mathbf{p}_{ij} = \frac{1}{\Delta y}(\mathbf{p}_{i,j+\frac{1}{2}} - \mathbf{p}_{i,j-\frac{1}{2}}).$$

Further in the case of the system (3.10) with the source term present, we get

$$\mathbf{u}^{n,1} = \mathbf{u}^n, \tag{5.4a}$$

$$\mathbf{v}^{n,1} = \mathbf{v}^n + \frac{\Delta t}{\epsilon}(\mathbf{v}^{n,1} - \mathbf{F}(\mathbf{u}^{n,1})) + \frac{\Delta t}{\epsilon}\widetilde{\mathbf{S}}(\mathbf{u}^{n,1}), \tag{5.4b}$$

$$\mathbf{w}^{n,1} = \mathbf{w}^n + \frac{\Delta t}{\epsilon}(\mathbf{w}^{n,1} - \mathbf{G}(\mathbf{u}^{n,1})) + \frac{\Delta t}{\epsilon}\widetilde{\widetilde{\mathbf{S}}}(\mathbf{u}^{n,1}); \tag{5.4c}$$

$$\mathbf{u}^{(1)} = \mathbf{u}^{n,1} - \Delta t(\Delta_+^x \mathbf{v}^{n,1} + \Delta_+^y \mathbf{w}^{n,1}), \tag{5.4d}$$

$$\mathbf{v}^{(1)} = \mathbf{v}^{n,1} - \Delta t \mathbf{C}^2 \Delta_+^x \mathbf{u}^{n,1}, \tag{5.4e}$$

$$\mathbf{w}^{(1)} = \mathbf{w}^{n,1} - \Delta t \mathbf{D}^2 \Delta_+^y \mathbf{u}^{n,1}; \tag{5.4f}$$

$$\mathbf{u}^{n,2} = \mathbf{u}^{(1)}, \tag{5.4g}$$

$$\mathbf{v}^{n,2} = \mathbf{v}^{(1)} - \frac{\Delta t}{\epsilon}(\mathbf{v}^{n,2} - \mathbf{F}(\mathbf{u}^{n,2})) - \frac{2\Delta t}{\epsilon}(\mathbf{v}^{n,1} - \mathbf{F}(\mathbf{u}^{n,1})) - \frac{\Delta t}{\epsilon}\widetilde{\mathbf{S}}(\mathbf{u}^{n,2}) - \frac{2\Delta t}{\epsilon}\widetilde{\mathbf{S}}(\mathbf{u}^{n,1}), \tag{5.4h}$$

$$\mathbf{w}^{n,2} = \mathbf{w}^{(1)} - \frac{\Delta t}{\epsilon}(\mathbf{w}^{n,2} - \mathbf{G}(\mathbf{u}^{n,2})) - \frac{2\Delta t}{\epsilon}(\mathbf{w}^{n,1} - \mathbf{G}(\mathbf{u}^{n,1})) - \frac{\Delta t}{\epsilon}\widetilde{\widetilde{\mathbf{S}}}(\mathbf{u}^{n,2}) - \frac{2\Delta t}{\epsilon}\widetilde{\widetilde{\mathbf{S}}}(\mathbf{u}^{n,1}); \tag{5.4i}$$

$$\mathbf{u}^{(2)} = \mathbf{u}^{n,2} - \Delta t(\Delta_+^x \mathbf{v}^{n,2} + \Delta_+^y \mathbf{w}^{n,2}), \tag{5.4j}$$

$$\mathbf{v}^{(2)} = \mathbf{v}^{n,2} - \Delta t \mathbf{C}^2 \Delta_+^x \mathbf{u}^{n,2} \tag{5.4k}$$

$$\mathbf{w}^{(2)} = \mathbf{w}^{n,2} - \Delta t \mathbf{D}^2 \Delta_+^y \mathbf{u}^{n,2}; \tag{5.4l}$$

$$\mathbf{u}^{n+1} = \frac{1}{2}(\mathbf{u}^n + \mathbf{u}^{(2)}), \tag{5.4m}$$

$$\mathbf{v}^{n+1} = \frac{1}{2}(\mathbf{v}^n + \mathbf{v}^{(2)}), \tag{5.4n}$$

$$\mathbf{w}^{n+1} = \frac{1}{2}(\mathbf{w}^n + \mathbf{w}^{(2)}), \tag{5.4o}$$

It is important to note that no information about the eigensystem of the Jacobian of the non-linear flux is required, except an upper bound of the largest eigenvalue in modulus, in order to adjust the parameter in **C** and **D** according to the subcharacteristic condition. In the relaxation context the characteristic variables are defined by a global transformation unlike the characteristic variables of the non-linear conservation law. The characteristic variables are still much simpler than those of the non-linear conservation law, since the relaxation system has linear characteristic variables $\mathbf{v} \pm \mathbf{Cu}$ and $\mathbf{w} \pm \mathbf{Du}$. It is worth noting here that, using the above schemes neither linear algebraic equation nor non-linear source terms arise. In addition both first and second-order relaxation schemes are stable under a *CFL* condition

$$\max\left((\max_i c_i)\frac{\Delta t}{\Delta x}, (\max_i d_i)\frac{\Delta t}{\Delta y}\right) \leqslant 1. \tag{5.5}$$

In order to retain the TVD property (see [17,7,36]) a more strict restriction has to be imposed on the usual CFL condition, and that has been applied in the following section in order to calculate Δt

$$CFL = \max\left((\max_i c_i)\frac{\Delta t}{\Delta x}, (\max_i d_i)\frac{\Delta t}{\Delta y}\right) \leqslant \frac{1}{2}.$$

The time discretization in the limit when $\epsilon \to 0^+$ converges to the TVD Runge–Kutta schemes given in [34].

6. Numerical tests and results

In this section we present some classical numerical tests and the obtained results that demonstrate and validate the performance of the relaxation schemes presented for the 2D SWEs. In all computations presented here the value of the CFL number used was set to 0.5.

6.1. Initial and boundary conditions

We choose the initial conditions for all the relaxation systems presented above as

$$\begin{aligned}
&\mathbf{u}(x,y,0) = \mathbf{u}_0(x,y),\\
&\mathbf{v}(x,y,0) = \mathbf{v}_0(x,y) \equiv \mathbf{F}(\mathbf{u}_0(x,y)),\\
&\mathbf{w}(x,y,0) = \mathbf{w}_0(x,y) \equiv \mathbf{G}(\mathbf{u}_0(x,y)).
\end{aligned}$$

In the small relaxation limit ($\epsilon \to 0^+$) the relaxation systems presented here satisfy the local equilibriums, and by choosing the above for **v** and **w** we avoid the introduction of an initial layer through the relaxation system.

For the boundary conditions given the physical boundary conditions, $\mathbf{u}_b$, that should imposed for each problem (transmissive or reflective in the following test problems), then we set $\mathbf{v}_b = \mathbf{F}(\mathbf{u}_b)$ and $\mathbf{w}_b = \mathbf{G}(\mathbf{u}_b)$ as to avoid the introduction of artificial boundary layers. In general, any choice that leads at the limit to the associated boundary and initial equilibrium can be used.

In practice, the choices of c_k, d_k, $k = 1, 2, 3$, in all the numerical tests are based on rough estimates of the eigenvalues $(u_1, u_1 \pm \sqrt{gh})$ and $(u_2, u_2 \pm \sqrt{gh})$ of the Jacobian matrices $\partial\mathbf{F}(\mathbf{u})/\partial\mathbf{u}$ and $\partial\mathbf{G}(\mathbf{u})/\partial\mathbf{u}$, respectively, of the original SWEs, as to satisfy the subcharacteristic condition (3.11). Another choice is to calculate c and d locally at every cell as

$$c_{i+\frac{1}{2},j} = \max_{u\in\{u_{i+\frac{1}{2},j}, u_{i-\frac{1}{2},j}\}} |\, \partial\mathbf{F}(u)/\partial u_k \,|, \quad d_{i,j+\frac{1}{2}} = \max_{u\in\{u_{i,j+\frac{1}{2}}, u_{i,j-\frac{1}{2}}\}} |\, \partial\mathbf{G}(u)/\partial u_k \,| .$$

A global choice is simply to take the maximum over the grid points as

$$c_k = d_k = \max_{i,j}(c_{i+\frac{1}{2},j}, d_{i,j+\frac{1}{2}}).$$

Other choices can be made as long as numerical stability is maintained. It should be noted here that larger values for the c_k, d_k, usually add more numerical viscosity, so for accuracy reasons it is desirable to have the c_k, d_k as small as possible. The first choice for calculating the characteristic speeds was proven sufficient for our calculations, although it is an interesting area of numerical analysis which could benefit from further investigation.

The relaxation parameter ϵ should be small with respect to the time step and space mesh length, that is $\Delta t \gg \epsilon$ and $\Delta y, \Delta x \gg \epsilon$. Again here, ϵ plays the role of viscosity coefficient so more numerical diffusion will be added for relatively larger values of ϵ.

Next, two typical examples of 2D dam-break problems are solved and discussed by solving the SWEs using the above relaxation scheme.

6.2. 2D partial dam-break

The first two-dimensional hypothetical problem is the one presented in [15]. The aim of this test case is to study the capability of the schemes to simulate different front wave propagations, with particular attention to the 2D aspects of the flow when different options (e.g. limiters) are used.

For this problem the dam, located in the center of a region, is assumed to partially fail instantaneously. The bottom is frictionless ($n_m = 0$). The water depth upstream of the dam is $h_u = 10$ m and downstream is assumed to be either $h_d = 5, 0.1, 0$ m (dry). Small (or even dry) downstream depths consist more severe tests for a numerical scheme. The computational domain is a 200 m × 200 m region which has been subdivided into 41×41 square grid. The breach is 75 m in length, which has distances of 30 m from the left bank and 95 m from the right. The boundary conditions at $x = 0$ and $x = 200$ m are assumed to be transmissive and all other boundaries are considered as reflective. At the instant of breaking of the dam, water is released through the breach, forming a positive wave propagating downstream and a negative wave spreading upstream. When $h_d = 5$ m the flow is subcritical everywhere.

The results after $t = 7.2$ s for the upwind relaxation scheme are shown in Fig. 1 in terms of water depth, contour of depth and velocity field, respectively. The computational parameters used were $\epsilon = 10^{-6}$ and $c_1 = 10$, $c_2 = 6$, $c_3 = 11$, $d_1 = 10$, $d_2 = 5$, $d_3 = 11$. The improvements in resolution and the calculation of fine details of the flow, when compare the results with the second-order MUSCL scheme in Fig. 2 with the MM limiter, can be clearly seen. The differences of applying different limiters to the MUSCL scheme can be seen when compare with the results obtained in Fig. 3 using the SB limiter, and the same computational parameters.

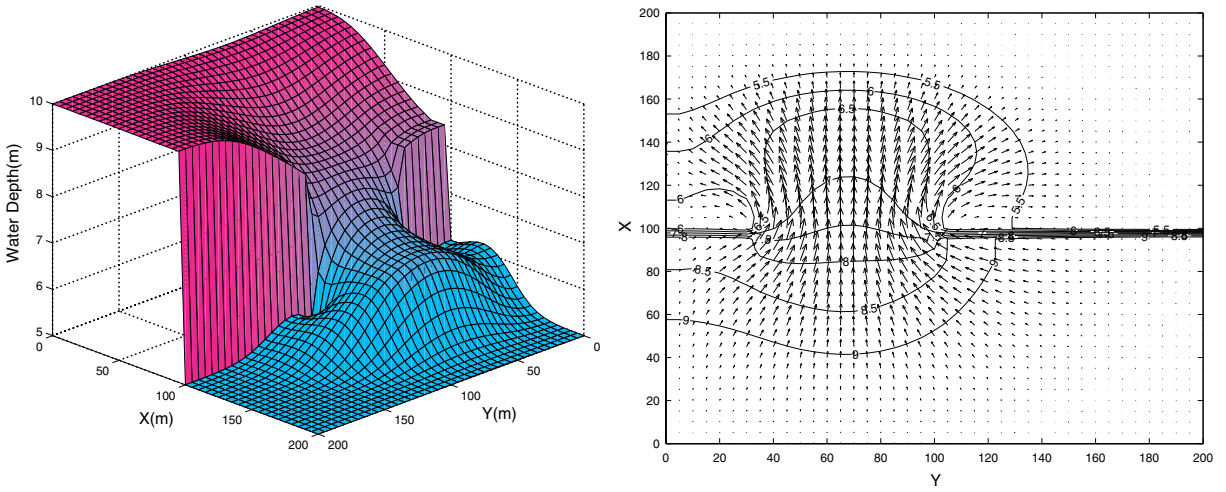

Fig. 1. Water depth and depth contours with the velocity field, for the partial dam-break flow ($h_d = 5$ m) at $t = 7.2$ s computed with the upwind relaxation scheme.

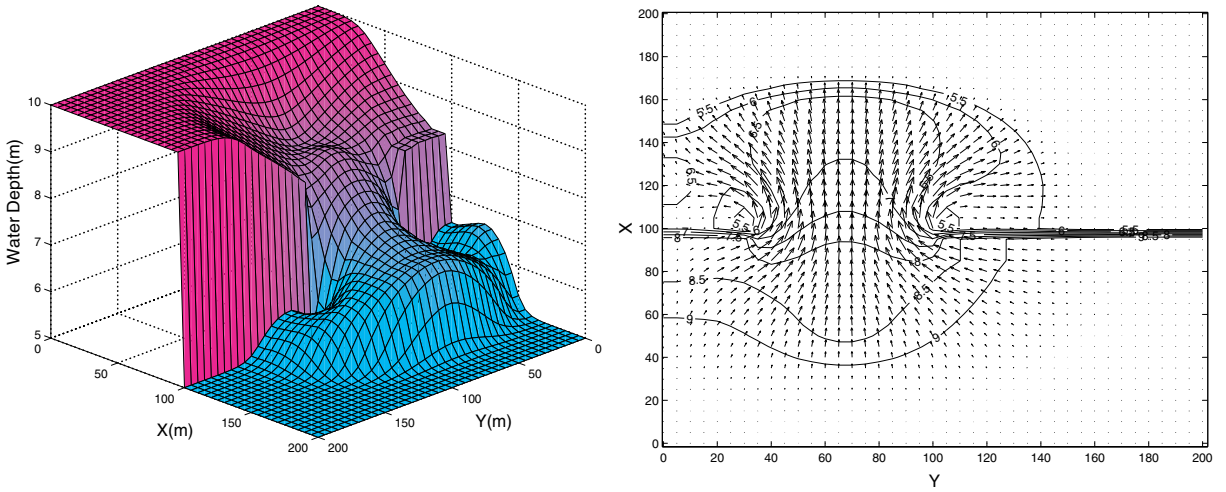

Fig. 2. Water depth and depth contours with the velocity field, for the partial dam-break flow ($h_d = 5$) at $t = 7.2$ s computed with the MUSCL relaxation scheme (MM limiter).

There is no analytical reference solution for this test case, but in the literature numerical results of various authors are available (e.g. [15,1,28,29,43,40]) The behavior of the relaxation schemes is in satisfactory agreement with computed results of these authors.

When there is a finite water depth downstream, a shock front always exists, see Fig. 4. This is not the case for the dry bed case. In the dry bed case the bore propagates much faster and at time $t = 7.2$ s has reached out to the computational domain boundary. There is also a significant difference in the velocity vector field in the two cases, see Fig. 5. Dealing with dry regions during the

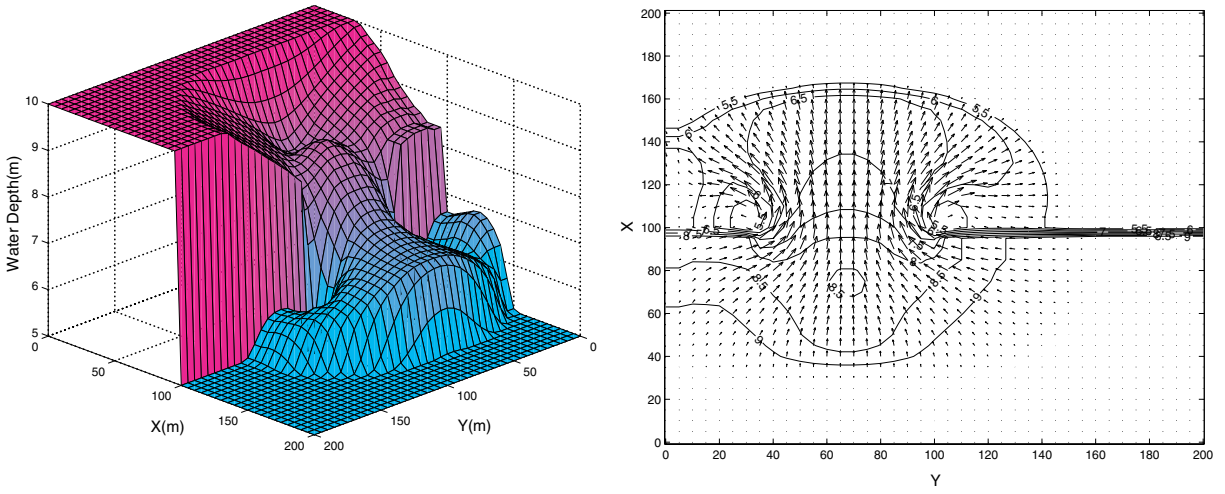

Fig. 3. Water depth and depth contours with the velocity field, for the partial dam-break flow ($h_d = 5$) at $t = 7.2$ s computed with the MUSCL relaxation scheme (SB limiter).

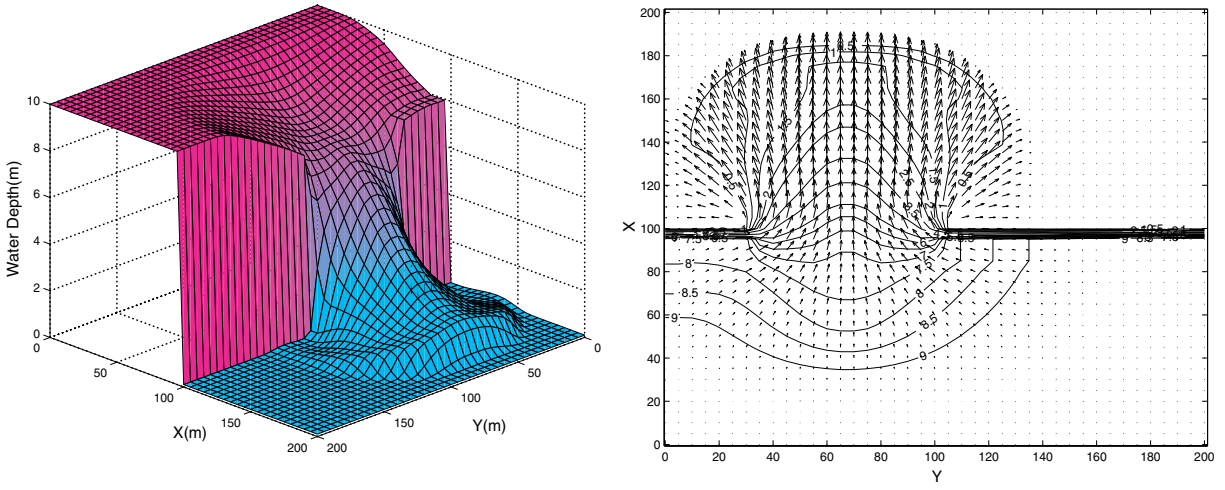

Fig. 4. Water depth and depth contours with the velocity field, for the partial dam-break ($h_d = 0.1$ m) at $t = 7.2$ s computed with the MUSCL relaxation scheme (VL limiter) ($c_1 = c_2 = 12, c_3 = 15, d_1 = d_3 = 12$, $d_2 = 6$).

computational process one or more eigenvalues might vanish. Consequently, the estimation of the characteristic speeds needed for the relaxation system is not valid anymore. In order to overcome this difficulty and treat dry cells in the computational domain, we perturbed the values of **C** and **D** by adding a threshold 10^{-3} to these characteristic speeds whenever they vanish. In the relaxation method no modifications have been incorporated to either the spatial discretizations or the IMEX time integration scheme. We point out that, the fact that one can resolve dry areas without

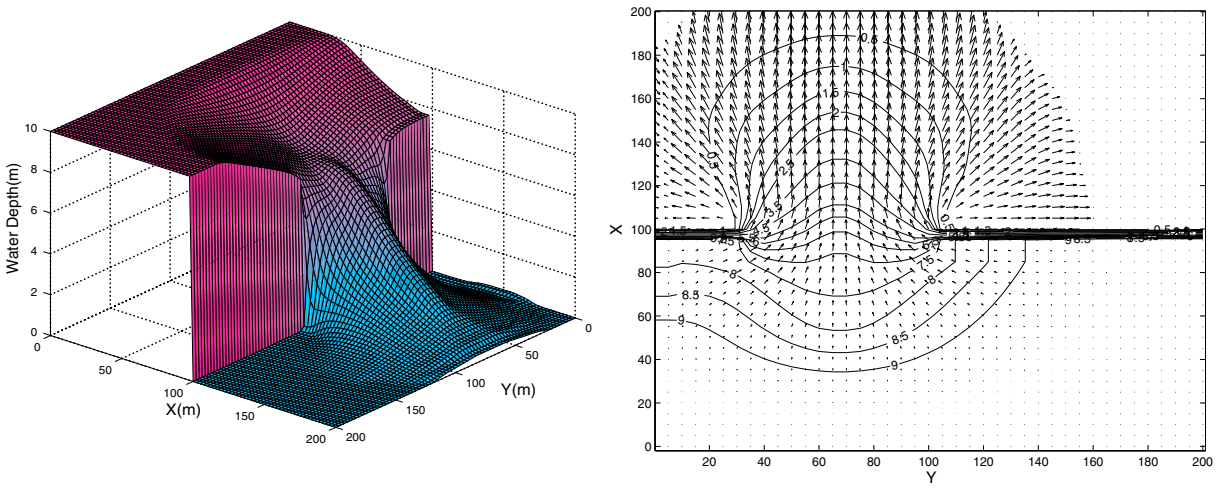

Fig. 5. Water depth and depth contours with the velocity field, for the partial dam-break ($h_d = 0$ m) at $t = 7.2$ s computed with the MUSCL relaxation scheme (VL limiter) ($c_1 = c_2 = 12$, $c_3 = 15$, $d_1 = d_3 = 12$, $d_2 = 10$).

modification of the scheme is due to the positivity preserving property of the scheme. We refer for example to [32] where further discussions on positivity-preserving property for the relaxation schemes can be found.

In the wet bed cases although there is a finite water depth downstream the flow velocity vanishes. In the dry case, the water depth is extremely small. We use an 81×81 grid to calculate the solution in the dry case shown in Fig. 5, that was proven more stable to capture the fine details of the flow. In the numerical scheme, h and q are the calculated variables. Machine precision will produce finite values for the dependant variable u, calculated as $u = q/h$, even though to machine precision h is considered as zero, see [43]. The results in Figs. 4 and 5 compare well with others found in the literature.

6.3. Circular dam-break in 2D

Another benchmark example is the one presented in [1]. It involves the breaking of a circular dam, and it is an important test example for the analysis and performance of the presented algorithms when solving complex shallow flow problems, especially for symmetry. Initially, the physical model is that of two regions of still water separated by a cylindrical wall (with radius 11 m) centered in a 50×50 m square domain. The water depth within the cylinder is 10 m and 1 m outside. The wall is then assumed to be removed completely and no slope or friction is considered. This is like a two dimensional Riemann problem for the 2D SWEs. The circular dam-break bore waves will spread and propagate radially and symmetrically as the water drains from the deepest region. Then there is a transition from subcritical to supercritical flow.

The results after $t = 0.69$ s (calculated in a 51×51 grid) are shown and compared for the different spatial accuracy and limiters used in Figs. 6–10, in terms of water depth, contour of depth and velocity field, respectively. The computational parameters used were $\epsilon = 10^{-6}$ and $c_1 = c_3 = 12, c_2 = 7, d_1 = d_3 = 12, d_2 = 7$.

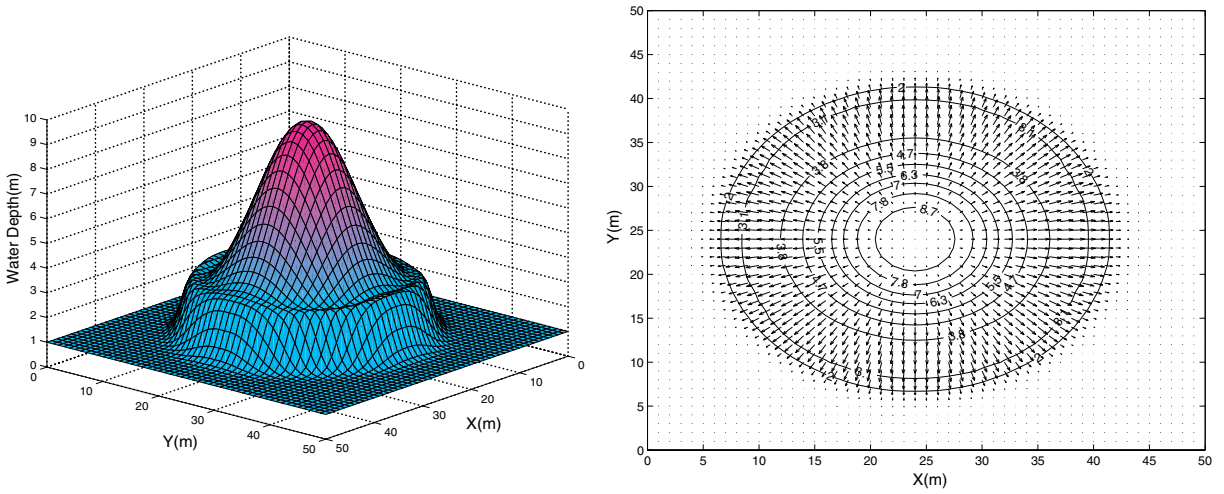

Fig. 6. Water depth and depth contours with the velocity field, at $t = 0.69$ s for the circular dam-break flow computed with the upwind relaxation scheme.

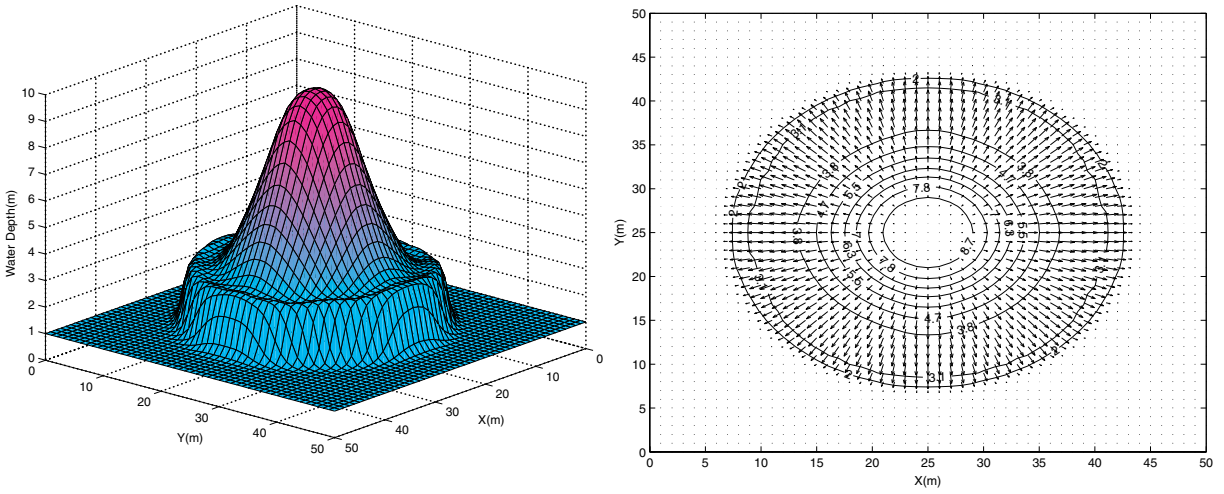

Fig. 7. Water depth and depth contours with the velocity field, at $t = 0.69$ s for the circular dam-break flow computed with the MUSCL relaxation scheme (MM limiter).

It can be clearly seen that the waves spread uniformly and symmetrically, with the radial symmetry slightly distorted by the effects of the grid due to the inability to represent a circle on a square grid, but otherwise the solution is very accurate and agrees very well with those presented for example in [1,28,29]. The second-order relaxation scheme produces sharp resolution of the abrupt changes. In all the results, there are small secondary waves (produced from the interaction of the initial discontinuity with that of the representation of the circle) which vanish as the solution evolves. The influence of the slope limiters used for the simulation can be seen comparing

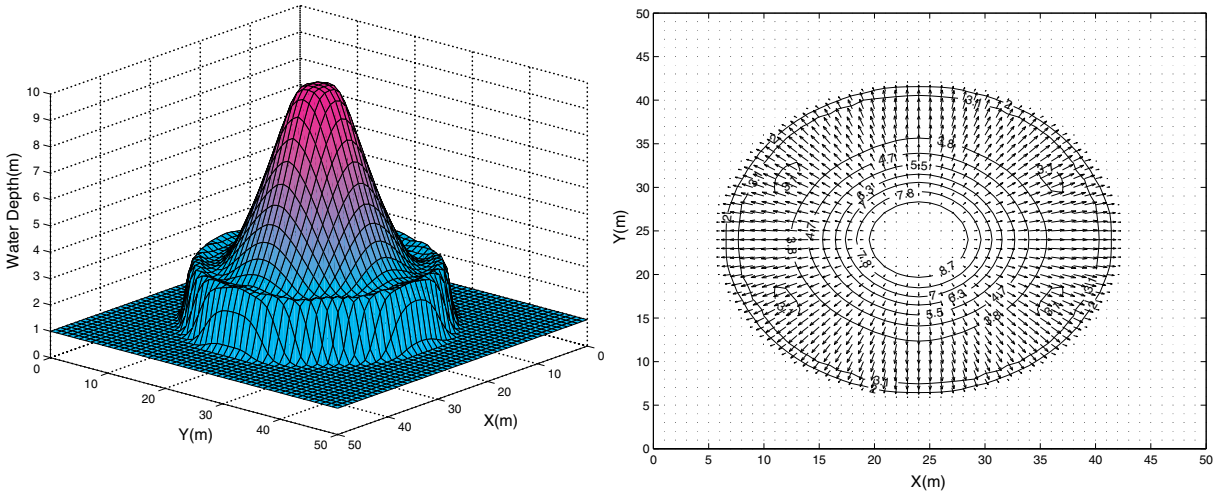

Fig. 8. Water depth and depth contours with the velocity field, at $t = 0.69$ s for the circular dam-break fl ow computed with the MUSCL relaxation scheme (VL limiter).

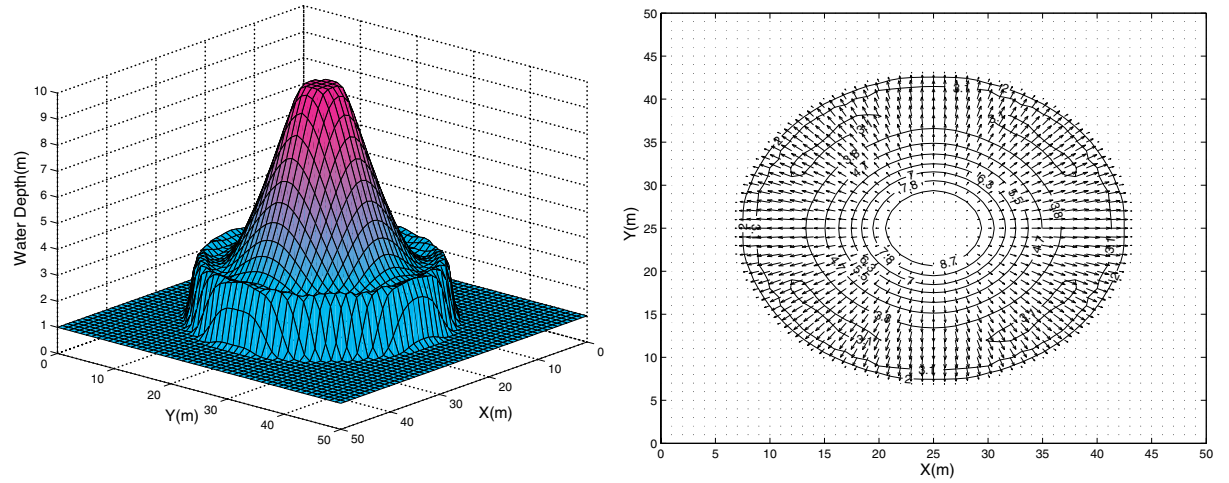

Fig. 9. Water depth and depth contours with the velocity field, at $t = 0.69$ s for the circular dam-break flow computed with the MUSCL relaxation scheme (MC limiter).

Figs. 7–10. As for the partial dam case, the MM limiter introduces the greatest diffusion smoothing the solution. The SB limiter produces the sharpest resolution. Similar observations were made in [43].

The case of an initially dry bed outside the cylinder is also considered here and presented in Fig. 11 for the MUSCL relaxing scheme with the VL limiter used in a 81×81 grid. It can be seen that no bore forms, instead a rarefaction wave extends into the dry region. The scheme is capable of

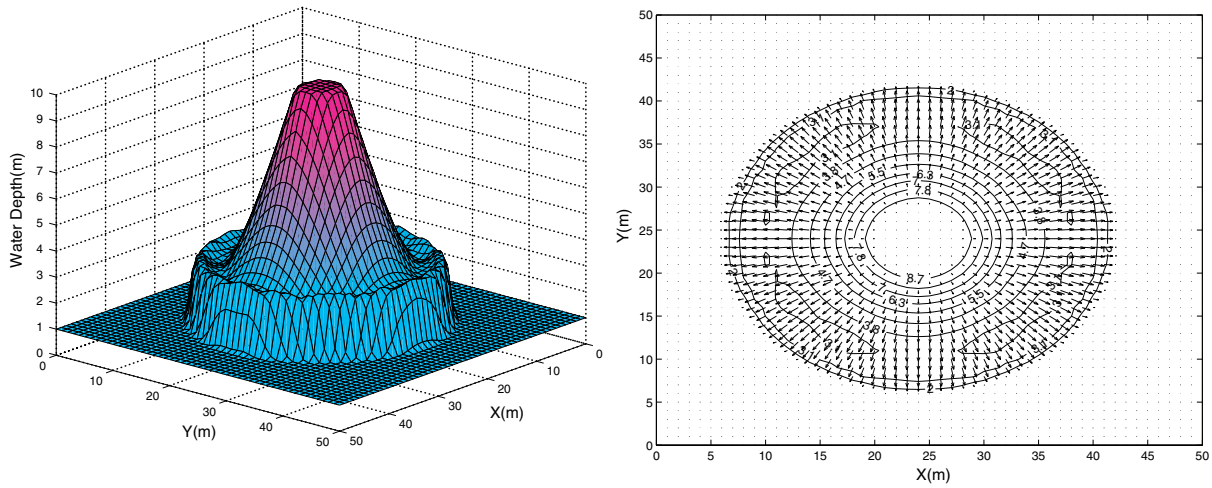

Fig. 10. Water depth and depth contours with the velocity field, at $t = 0.69$ s for the circular dam-break flow computed with the MUSCL relaxation scheme (SB limiter).

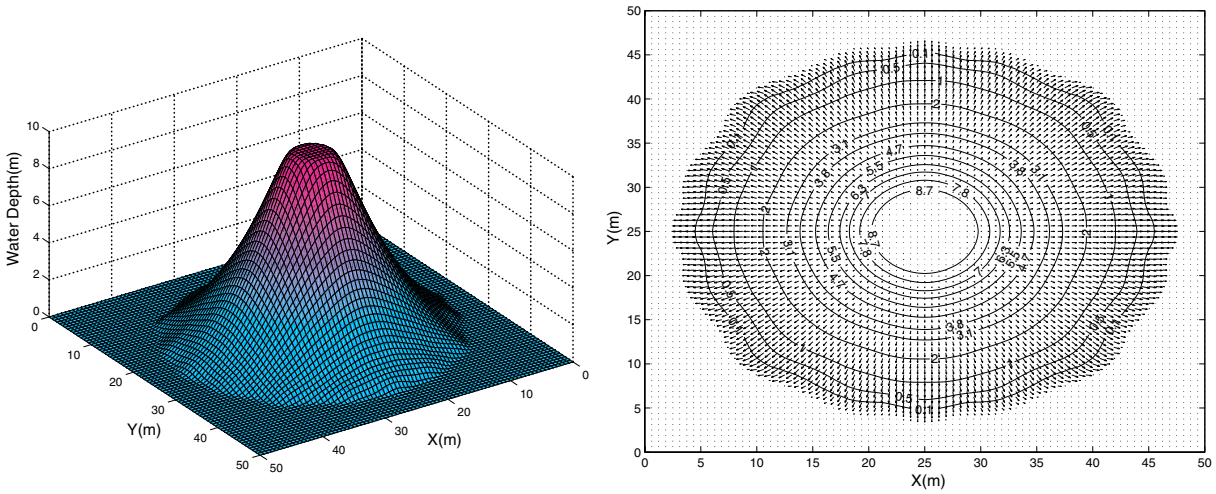

Fig. 11. Water depth and depth contours with the velocity field, at $t = 0.69$ s for the dry bed circular dam-break flow computed with the MUSCL relaxation scheme (VL limiter).

handling the dry bed problem. The computational parameters used for this problem were $\epsilon = 1\text{E}{-}6$ and $c_1 = c_3 = 12.5$, $c_2 = 10$,$d_1 = d_3 = 12.5$, $d_2 = 10$.

6.3.1. Toro's reference solution

This is a test problem similar to the one presented above, and it was discussed in [37]. We consider a circular dam of radius 2.5 m in the center of a 40 m × 40 m square domain, with the water depth within the dam set at 2.5 m high and 0.5 m outside. We apply the MUSCL relaxation

scheme using the SB limiter in all computations. The computational parameters used were $\epsilon = 10^{-6}$, $c_1 = c_3 = 5$, $c_2 = 2$, $d_1 = d_3 = 5$, $d_2 = 2$. We have used a fine mesh of 201×201 cells, as to be consistent with that used to calculate the reference solution in [37]. The purpose of this test is to compare our results with those produced in [37] using other well establish methods, in order to study the wave propagation phenomena associated with this problem.

In Fig. 12, where the water depth profile is shown for time $t = 0.4$ s on the left, an outward-propagating circular shock and an inward-propagating circular rarefaction wave can be clearly seen. At this time the rarefaction is about to reach the center of the dam. At time $t = 0.7$ s (Fig. 12 on the right) the circular rarefaction has by now imploded into the center and has

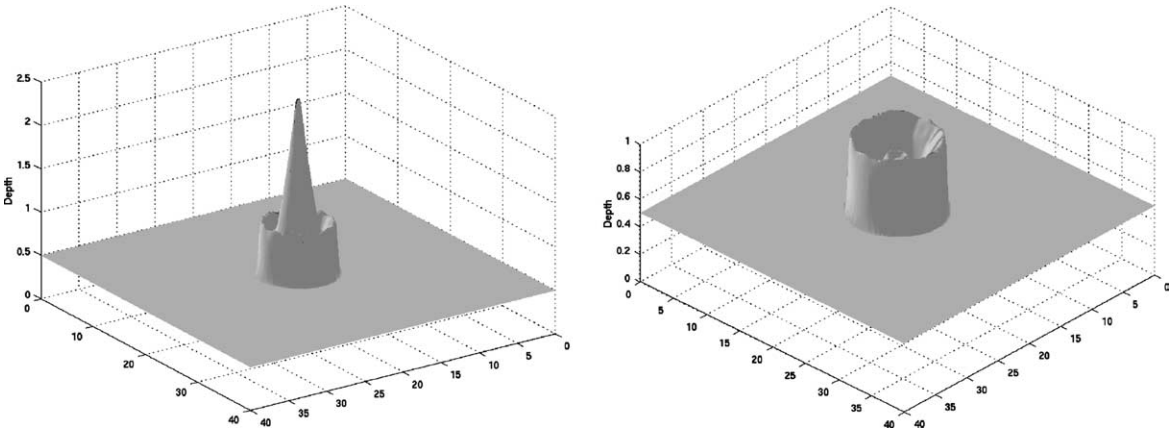

Fig. 12. Circular dam-break water depth at times $t = 0.4$ s (left) and $t = 0.7$ s (right).

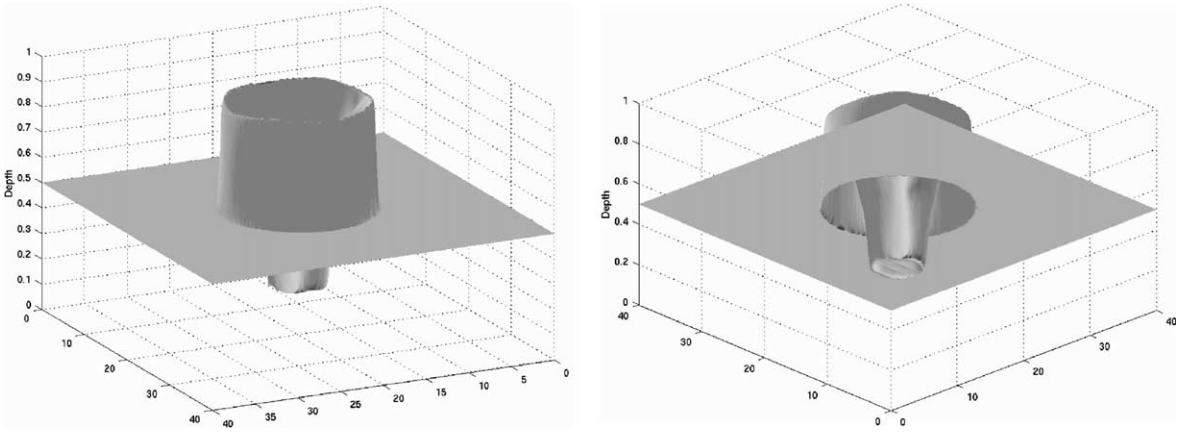

Fig. 13. Circular dam-break water depth at times $t = 1.4$ s side view (left) and bottom view (right).

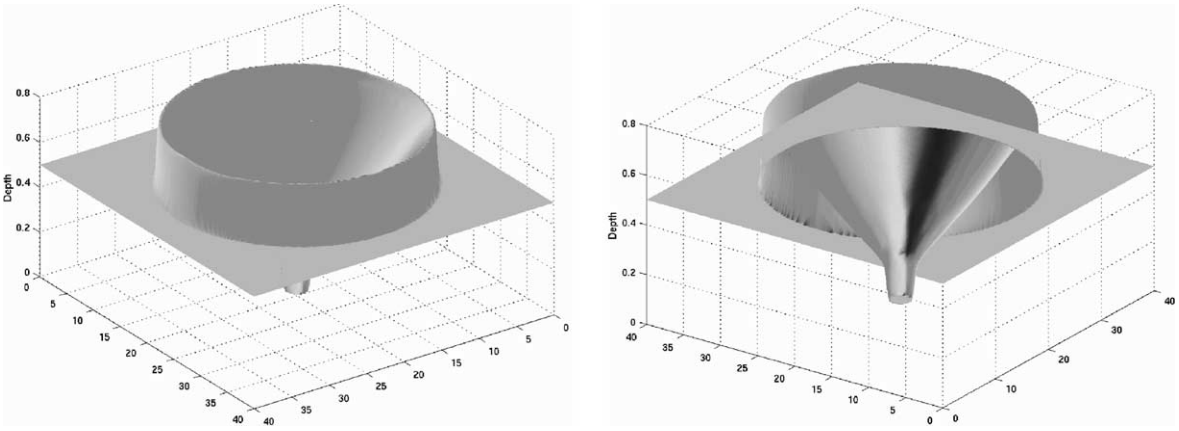

Fig. 14. Circular dam-break water depth at times $t = 3.5$ s top view (left) and bottom view (right).

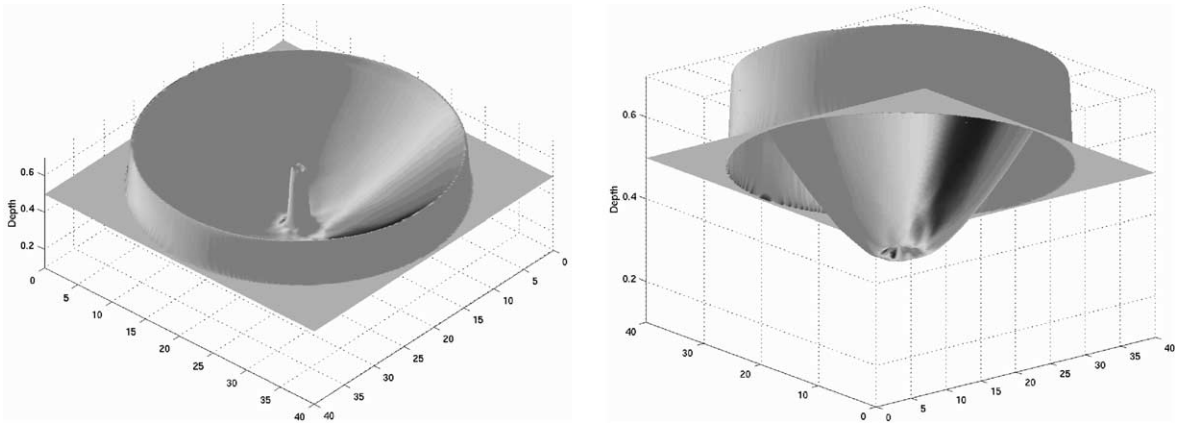

Fig. 15. Circular dam-break water depth at times $t = 4.7$ s top view (left) and bottom view (right).

reflected producing a very pronounced fall of the water depth right in the center. As mentioned in [37] this feature is difficult to resolve numerically.

In Fig. 13 the water depth is displayed at time $t = 1.4$ s. Here the circular shock has propagated further outwards and the reflected inner circular rarefaction has overexpanded the flow to the point that the free surface position has fallen below the initial water depth of 0.5 m outside the dam, producing a secondary circular shock below this depth as can be seen from the bottom view in Fig. 13 on the right.

Fig. 14 shows the corresponding top and bottom view of the water depth at time $t = 3.5$ s, where the primary circular shock has propagated further away from the center and the secondary circular shock has propagated towards the center. Fig. 15 shows a top and bottom view of the

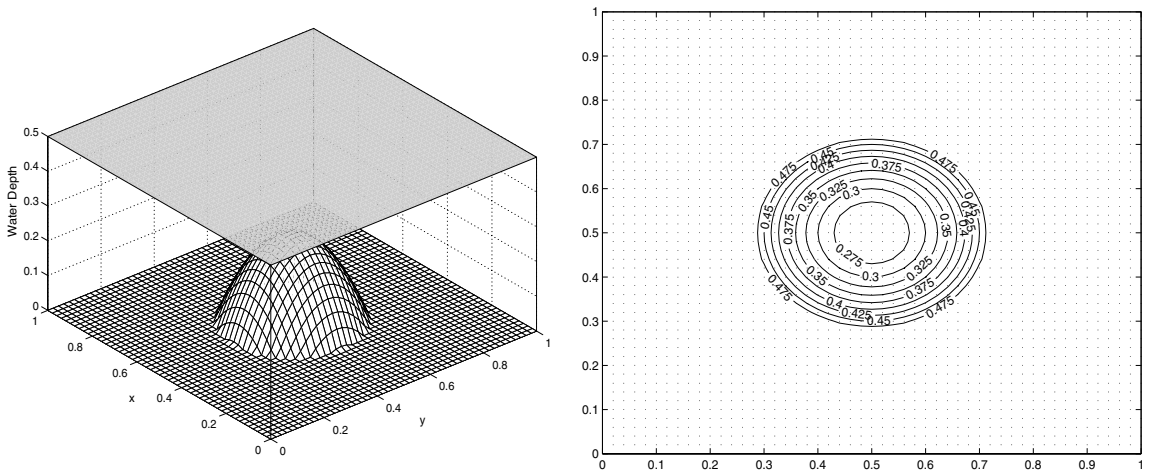

Fig. 16. Water depth over a bump and depth contours with velocity field, for a steady flow over a bump.

water depth at time $t = 4.7$ s, which is shortly after the secondary shock has imploded into the center. This shock has reflected from the center and is now propagating outwards.

All the results presented in Figs. 12–15 are in perfect agreement with those presented in [37], where this problem has been extensively studied.

6.4. Steady flow over a hump

As a first problem with a source term present we consider the academic test case, presented in [5], of a 1 m × 1 m square pool with a symmetric hump situated at the center presented in [5]. The pool is assume totally closed by solid vertical walls. The bump is mathematically defined by

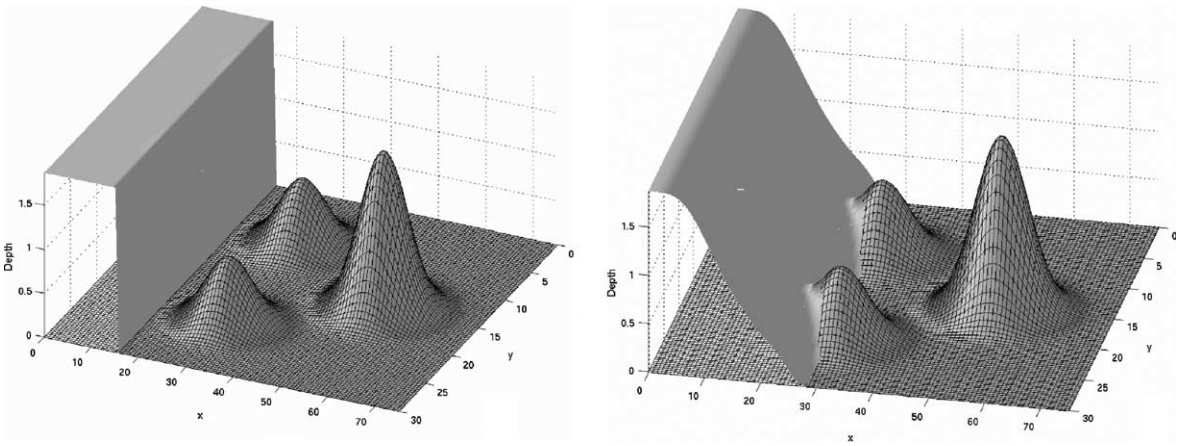

Fig. 17. Water depth propagation at $t = 0$ s (left) and $t = 2$ s (right).

$$Z = \max\left[0, \frac{1}{4} - 5\left(\left(x - \frac{1}{2}\right)^2 + \left(y - \frac{1}{2}\right)^2\right)\right].$$

Initial conditions covering totally the bump are $h + Z = 0.5$ m,$u_1 = u_2 = 0$ m/s. The flow evolves during 60 s and the initial steady-state must be preserved. The results for scheme (3.10) (that was proven in [14] more accurate for similar 1D problems when compared to scheme (3.7)) are presented in Fig. 16. A uniform 51×51grid was used and the computational parameters were $\epsilon = 10^{-8}$ and $c_1 = c_3 = 2.5$, $c_2 = 0.5$, $d_1 = d_3 = 2.5$, $d_2 = 0.5$. The steady-state is correctly maintained. The overall equilibrium is conserved with no unphysical velocities appearing in the results that would alter the steady-state.

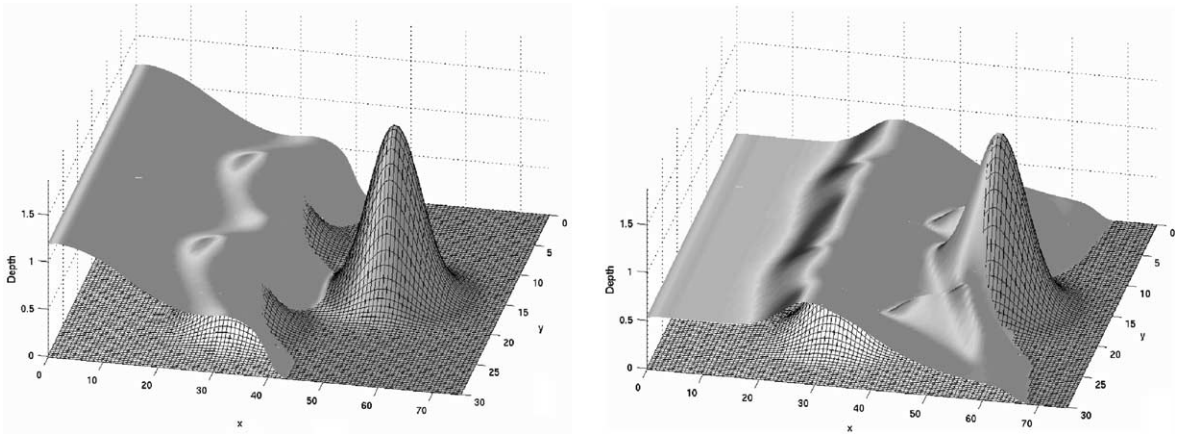

Fig. 18. Water depth propagation at $t = 5$ s (left) and $t = 10$ s (right).

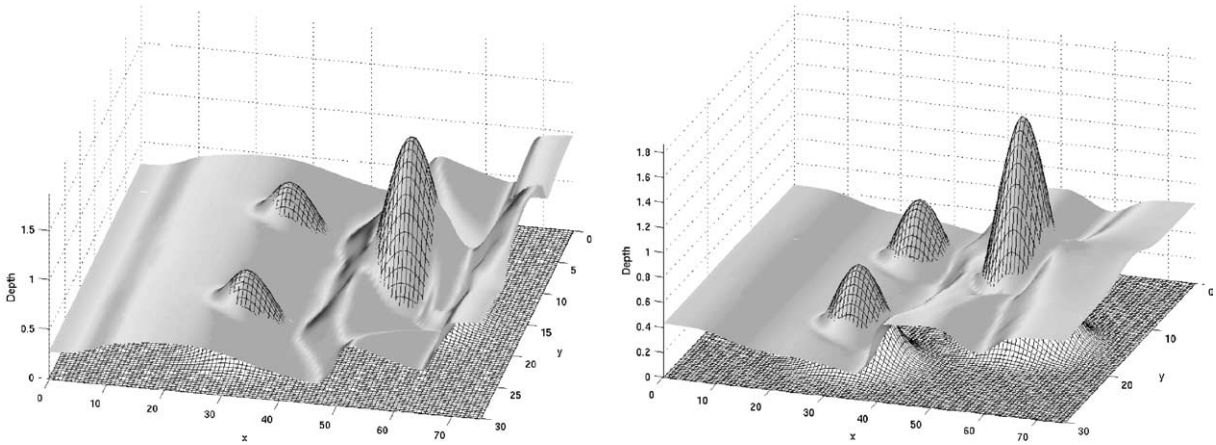

Fig. 19. Water depth propagation at $t = 20$ s (left) and $t = 30$ s (right).

6.5. Dam-break in a channel with topography and friction

In this test case, the performance of the relaxation scheme as to calculate more realistic situations is validated. The problem is similar to that presented in Refs. [5,6]. In a channel 75 m long and 30 m wide the dam is situated at $x = 16$ m with initial water depth $h + Z = 1.875$ m while the rest of the channel is considered dry. Three mounds are located in the channel bottom. The initial condition and the channel geometry can be seen in Fig. 17 on the left. The Manning coefficient $n_{\mathrm{m}} = 0.018$ for this problem. Boundary fixed conditions are solid walls. The computational parameters used were $\epsilon = 10^{-8}$, $c_i = d_i = 5$, $i = 1, 2, 3$, with the application of the MC limiter.

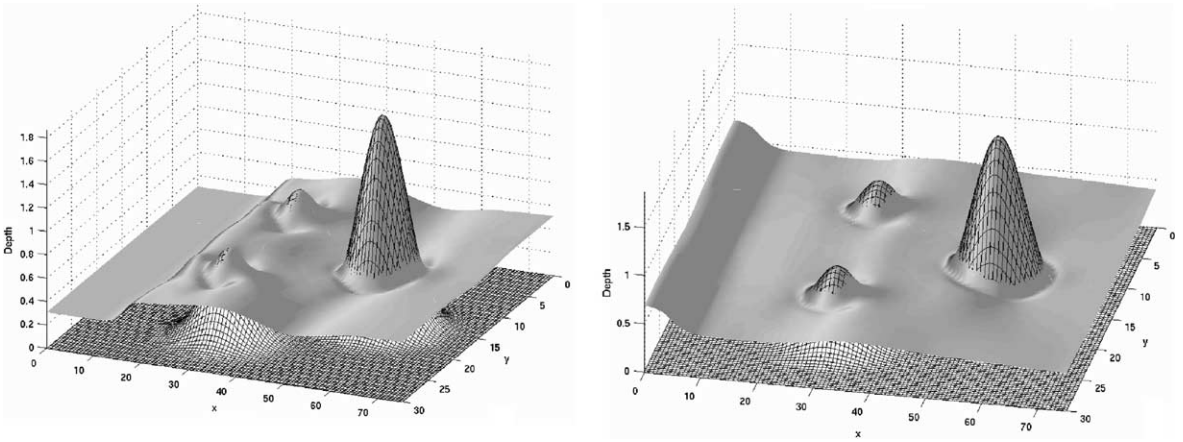

Fig. 20. Water depth propagation at $t = 40$ s (left) and $t = 50$ s (right).

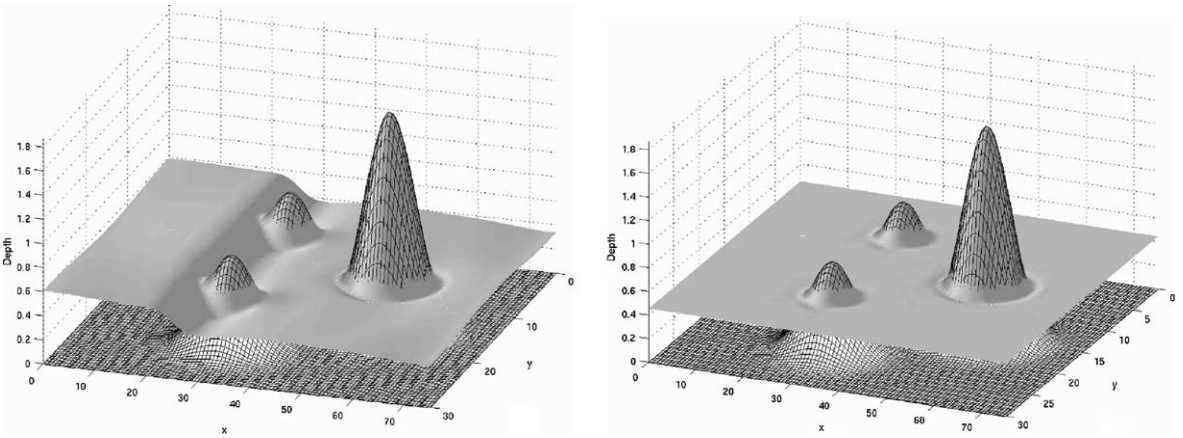

Fig. 21. Water depth propagation at $t = 60$ s (left) and $t = 400$ s (right).

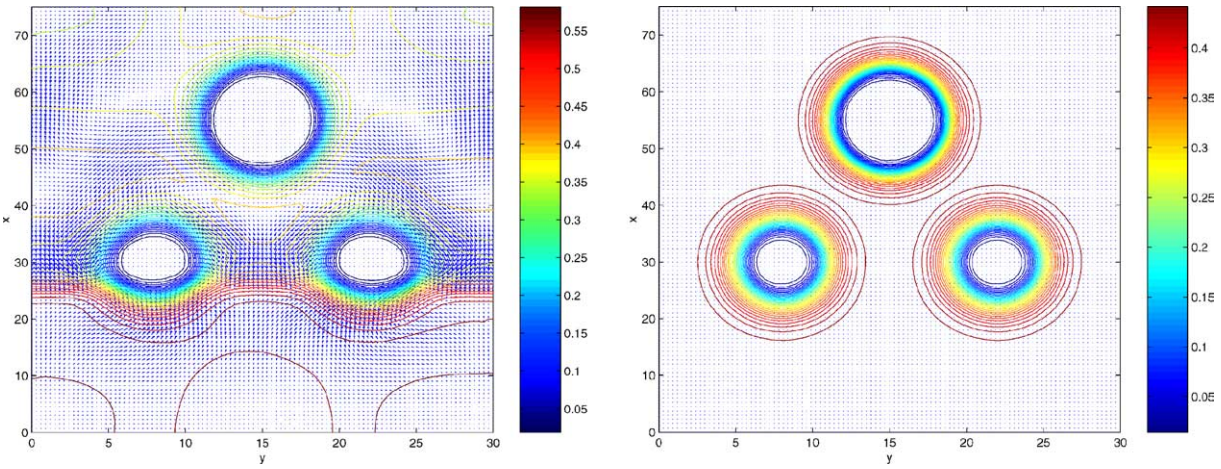

Fig. 22. Contour plots for the water depth propagation with the velocity field at $t = 60$ s (left) and $t = 400$ s (right).

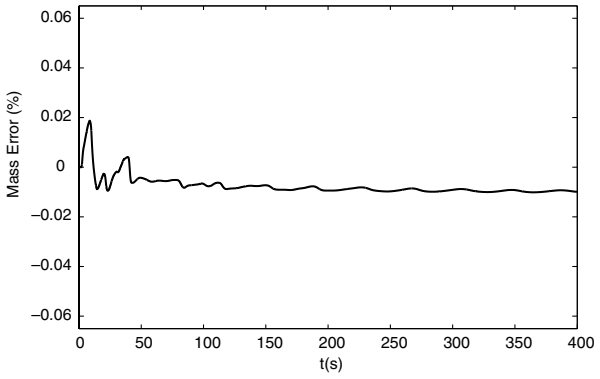

Fig. 23. Mass error time evolution during the computation.

Numerical results are presented in Figs. 17–21 for water depth at different times to show the propagation of the flood until steady-state is reached. The small mounds are covered by the water in its propagation and the effect of advancing and recession over the sloppy bed is clear. The higher mound is always almost dry and the accumulation of water can be clearly observed. The collision of the advancing front first with the higher mound and then with the downstream boundary wall can be seen having the expected physical behavior. The generation of dry bed can also be observed for the small mounds as time evolves until it reaches a steady-state. The contour plots for h, along with the velocity field, at times $t = 60$ s and $t = 400$ s are also presented in Fig. 22, where one can clearly see the final state state solution. The time evolution of the mass error calculated, as in [6], taking into account the initial mass volume (V_I) and the mass volume at each time step (V_n), in the form

$$\text{Mass Error}(\%) = \frac{V_n - V_I}{V_I}$$

is also presented in Fig. 23 where it is clear that the scheme is highly conservative, with small conservation error even when advance takes place over the initially dry bed.

7. Conclusions

In the present work relaxation schemes have been studied in order to compute numerical solutions for the two dimensional shallow water flows with and without source terms present. The main feature of the schemes is their simplicity and robustness. Finite volume shock capturing spatial discretization, that are Riemann solver free, have been used providing accurate shock resolution. Novel ways to incorporate the topography source term were applied with the relaxation model and only small errors were introduced while preserving steady-states. From theoretical point of view, the reconstruction proposed in the paper for relaxation system can be extended to the SWEs with space dependent flux and Coriolis forces. All what the relaxation methods require is the correct local equilibrium used to recover the original system when $\epsilon \to 0$. Once the local equilibrium is given, initial and boundary conditions for the relaxation system can be easily reconstructed, and an accurate selection of the characteristic speeds can also be estimated. The benchmark tests have shown that the schemes provide accurate solutions in good agreement with well documented ones. Though comparable resolutions with other well established methods are offered, the relaxation schemes have simplicity as their main advantage. The results also demonstrate that relaxation schemes are accurate, efficient and robust and can be of practical consideration and further development when solving shallow water flow problems.

References

[1] F. Alcrudo, P. Garcia-Navarro, A high resolution Godunov-type scheme in finite volumes for the 2D shallow water equations, Int. J. Numer. Methods Fluids 16 (1993) 489–505.
[2] D. Aregba-Driollet, R. Natalini, Convergence of relaxation schemes for conservation laws, Appl. Anal. 61 (1996) 163–193.
[3] Ch. Arvanitis, Th. Katsaounis, Ch. Makridakis, Adaptive finite element relaxation schemes for hyperbolic conservations laws, M2AN 35 (2001) 17–33.
[4] A. Bermudez, A. Dervieux, J.A. Desideri, M.E. Vazquez, Upwind schemes for the two-dimensional shallow water equations with variable depth using unstructured meshes, Comput. Methods Appl. Mech. Eng. 155 (1998) 49–72.
[5] P. Brufau, P. Garcia-Navarro, Unsteady free surface flow simulation over complex topography with a multidimensional upwind technique, J. Comp. Phys. 186 (2003) 503–526.
[6] P. Brufau, M.E. Vázquez-Céndon, P. Garcia-Navarro, A numerical model for the flooding and drying of irregular domains, Int. J. Numer. Methods Fluids 39 (2002) 247–275.
[7] A. Chalabi, Convergence of relaxation schemes for hyperbolic conservation laws with stiff source terms, Math. Comput. 68 (1999) 955–970.
[8] A. Chalabi, D. Seghir, Convergence of relaxation schemes for initial boundary value problems for conservation laws, Comp. Math. Appl. 43 (2002) 1079–1093.
[9] G.O. Chen, T.P. Liu, Zero relaxation and dissipation limits for hyperbolic conservation laws, Commun. Pure Appl. Math. 46 (1993) 744–781.

[10] G.O. Chen, C.D. Levermore, T.P. Liu, Hyperbolic conservation laws with stiff relaxation terms and entropy, Commun. Pure Appl. Math. 47 (1994) 787–830.
[11] A.I. Delis, Improved application of the HLLE Riemann solver for the shallow water equations with source terms, Commun. Numer. Methods Eng. 39 (2003) 59–83.
[12] A.I. Delis, C.P. Skeels, TVD schemes for open channel flow, Int. J. Numer. Methods Fluids 26 (1998) 791–809.
[13] A.I. Delis, C.P. Skeels, S.C. Ryrie, Implicit high-resolution methods for modelling one-dimensional open channel flow, J. Hydraul. Res. 40 (2000) 369–382.
[14] A.I. Delis, Th. Katsaounis, Relaxation schemes for the shallow water equations, Int. J. Numer. Methods Fluids 41 (2003) 695–719.
[15] R.J. Fennema, M.H. Chaudhry, Explicit methods for 2D transient free surface flows, J. Hydraul. Eng.-ASCE 116 (1990) 1013–1034.
[16] P. Garcia-Navarro, M.E. Vázquez-Cendón, On numerical treatment of the source terms in the shallow water equations, Comput. Fluids 29 (2000) 951–979.
[17] S. Jin, Z. Xin, The relaxing schemes of conservations laws in arbitrary space dimensions, Commun. Pure Appl. Math. 48 (1995) 235–277.
[18] S. Jin, C.D. Levermore, Numerical schemes for hyperbolic conservation laws with stiff relaxation terms, J. Comp. Phys 126 (1996) 449–467.
[19] Th. Katsaounis, Ch. Makridakis, Finite volume relaxation schemes for the multidimensional conservation laws, Math. Computat. 70 (2001) 533–553.
[20] Th. Katsaounis, Ch. Makridakis, Adaptive finite element relaxation schemes for the Saint-Venant system, in: T. Hou, E. Tadmor (Eds.), Hyperbolic Problems: Theory, Numerics, Applications, Springer, Berlin, 2003, pp. 621–631.
[21] M. Katsoulakis, G. Kossioris, Ch. Makridakis, Convergence and error estimates of relaxation schemes for multidimensional conservation laws, Commun. Part. Different. Equat. 24 (1999) 395–424.
[22] C. Lattanzio, D. Serre, Convergence of a relaxation scheme for hyperbolic systems of conservation laws, Numer. Math. 88 (2001) 121–134.
[23] R.J. LeVêque, M. Pelanti, A class of approximated Riemann solvers and their relation to relaxation schemes, J. Comput. Phys. 172 (2001) 572–591.
[24] R.J. LeVêque, Finite Volume Methods for Hyperbolic Problems, Cambridge University Press, Cambridge, 2002.
[25] T.P. Liu, Hyperbolic conservation laws with relaxation, Commun. Math. Phys. 108 (1987) 153–175.
[26] H.L. Liu, G. Warnecke, Convergence rates for relaxation schemes approximating conservation laws, SIAM J. Numer. Anal. 37 (2000) 1316–1337.
[27] M. Louaked, L. Hanich, TVD-multiresolution scheme for the shallow water equations, C.R. Acad. Sci. Paris Sr. I Math. 331 (2000) 745–750.
[28] M. Louaked, L. Hanich, TVD scheme for the shallow water equations, J. Hydraulic Res. (1998) 363–378.
[29] C.G. Mingham, D.M. Causon, High-resolution finite-volume method for shallow water flows, J. Hydraul. Eng.-ASCE 124 (1998) 605–614.
[30] R. Natalini, Convergence to equilibrium for the relaxation approximations of conservation laws, Commun. Pure Appl. Math. 49 (1996) 795–823.
[31] T.C. Rebollo, A.D. Delgado, E.D.F. Nieto, A family of stable numerical solvers for the shallow water equations with source terms, Comput. Methods Appl. Mech. Eng. 192 (2003) 203–225.
[32] L. Pareschi, G. Russo, Implicit–explicit Runge–Kutta schemes and applications to hyperbolic systems with relaxation, J. Sci. Comput., in press.
[33] H.J. Schroll, High resolution relaxed upwind schemes in gas dynamics, J. Scientific Computing 17 (2002) 599–607.
[34] C.-W. Shu, S. Osher, Efficient implementation of essentially nonoscillatory shock-capturing schemes, J. Comput. Phys. 77 (1988) 439–471.
[35] P.K. Sweby, High resolution schemes using flux limiters for hyperbolic conservation laws, SIAM J. Numer. Anal. 21 (1984) 995–1011.
[36] T. Tang, J. Wang, Convergence of MUSCL relaxing schemes to the relaxed schemes for conservation laws with stiff source terms, J. Sci. Comput. 15 (2000) 173–195.
[37] E.F. Toro, Shock-Capturing Methods for Free-Surface Shallow Flows, Wiley, New York, 2001.

[38] A.E. Tzavaras, Materials with internal variables and relaxation to conservation laws, Arch. Ration. Mech. Anal. 146 (1999) 129–155.
[39] M.E. Vázquez-Cendón, Improved treatment of source terms in upwind schemes for the shallow water equations in channels with irregular geometry, J. Comp. Phys. 148 (1999) 497–526.
[40] J.S. Wang, H.G. Ni, Y.S. He, Finite-difference TVD scheme for computation of dam-break problems, J Hydraul. Eng.-ASCE 126 (2000) 253–262.
[41] W.-C. Wang, Nonlinear stability of centered rarefaction waves of the Jin–Xin relaxation model for 2×2 conservation laws, Electron. J. Different. Equat. 57 (2002) 1–20.
[42] W.Q. Xu, Relaxation limit for piecewise smooth solutions to systems for conservation laws, J. Differen. Equat. 162 (2000) 140–173.
[43] C. Zoppou, S. Roberts, Numerical solution of the two-dimensional unsteady dam break, Appl. Math. Model. 24 (2000) 457–475.